EUROPEAN RESPIRATORY *journal*

FLAGSHIP SCIENTIFIC JOURNAL OF ERS

Early View

Original research article

Macrophage-derived IL-6 trans-signaling as a novel target in the pathogenesis of bronchopulmonary dysplasia

Dharmesh Hirani, Cristina M. Alvira, Soula Danopoulos, Carlos Milla, Michele Donato, Lu Tian, Jasmine Mohr, Katharina Dinger, Christina Vohlen, Jaco Selle, Silke v. Koningsbruggen-Rietschel, Verena Barbarino, Christian Pallasch, Stefan Rose-John, Margarete Odenthal, Gloria S. Pryhuber, Siavash Mansouri, Rajkumar Savai, Werner Seeger, Purvesh Khatri, Denise Al Alam, Jörg Dötsch, Miguel A. Alejandre Alcazar

Please cite this article as: Hirani D, Alvira CM, Danopoulos S, *et al*. Macrophage-derived IL-6 trans-signaling as a novel target in the pathogenesis of bronchopulmonary dysplasia. *Eur Respir J* 2021; in press (https://doi.org/10.1183/13993003.02248-2020).

Macrophage-derived IL-6 trans-signaling as a novel target in the pathogenesis of bronchopulmonary dysplasia

Dharmesh Hirani[1,2], Cristina M. Alvira[3], Soula Danopoulos[4], Carlos Milla[3], Michele Donato[5], Lu Tian[6], Jasmine Mohr[1,2], Katharina Dinger[1,2], Christina Vohlen[1,7], Jaco Selle[1], Silke v. Koningsbruggen-Rietschel[7], Verena Barbarino[8], Christian Pallasch[8], Stefan Rose-John[9], Margarete Odenthal[10], Gloria S. Pryhuber[11], Siavash Mansouri[12], Rajkumar Savai[12,13], Werner Seeger[12, 13], Purvesh Khatri[5], Denise Al Alam[4], Jörg Dötsch[7], Miguel A. Alejandre Alcazar[1,2,13,14]

[1]University of Cologne, Faculty of Medicine and University Hospital Cologne, Translational Experimental Pediatrics - Experimental Pulmonology, Department of Pediatric and Adolescent Medicine, Germany; [2]University of Cologne, Faculty of Medicine and University Hospital Cologne, Center for Molecular Medicine Cologne (CMMC), Germany; [3]Department of Pediatrics, Stanford University School of Medicine, Stanford, CA, USA; [4]Lundquist Institute for Biomedical Innovation at Harbor-UCLA Medical Center , Torrance, CA, United States; [5]Biomedical Informatics Research-Institute for Immunity, Transplantation, and Infection, Stanford University, Stanford, California; [6]Department of Biomedical Data Science, Stanford University, Stanford, USA; [7]University of Cologne, Faculty of Medicine and University Hospital Cologne, Department of Pediatric and Adolescent Medicine, Germany; [8]Department I of Internal Medicine, Center for Integrated Oncology (CIO) Köln-Bonn, University of Cologne, Germany, [9]Institute of Biochemistry, Christian-Albrechts-University Kiel, Germany; [10]University of Cologne, Faculty of Medicine and University Hospital Cologne, Institute for Pathology, Germany; [11]Division of Neonatology, Department of Pediatrics, University of Rochester Medical Center, Rochester, NY, USA. [12]Department of Lung Development and Remodeling, Max-Planck-Institute for Heart and Lung Research, Member of the German Center for Lung Research (DZL), Bad Nauheim, Germany; [13]Institute for Lung Health (ILH), University of Giessen and Marburg Lung Center (UGMLC), Member of the German Center for Lung Research (DZL), [14]University of Cologne, Faculty of Medicine and University Hospital Cologne, Cologne Excellence Cluster on Stress Responses in Aging-associated Diseases (CECAD), Cologne, Germany.

Summary: M1-like macrophage activation is linked to IL-6/STAT3 axis in clinical and experimental BPD. Inhibition of macrophage-related IL-6 trans-signaling promotes ATII survival and lung growth in experimental BPD as a new therapy for preterm infants.

Corresponding author: Miguel A. Alejandre Alcázar, M.D., Ph.D.
Assistant Professor (Translational Experimental Pediatrics)
Experimental Pulmonology
Department of Pediatrics and Adolescent Medicine
University of Cologne
Kerpener Strasse 62
D-50937 Cologne
Tel.: +49 (0)221 478 96876
Fax.: +49 (0)221 478 96868
Email: miguel.alejandre-alcazar@uk-koeln.de

All authors declare that there are no conflicts of interest concerning this study.

Abstract

Rationale: Premature infants exposed to oxygen are at risk for bronchopulmonary dysplasia (BPD), which is characterized by lung growth arrest. Inflammation is important, but the mechanisms remain elusive. Here, we investigated inflammatory pathways and therapeutic targets in severe clinical and experimental BPD.

Methods and Results: First, transcriptomic analysis with *in-silico* cellular deconvolution identified a lung-intrinsic M1-like-driven cytokine pattern in newborn mice after hyperoxia. These findings were confirmed by gene expression of macrophage-regulating chemokines (*Ccl2*, *Ccl7*, *Cxcl5*) and markers (*Il6*, *Il17A*, *Mmp12*). Second, hyperoxia-activated IL-6/STAT3 signaling was measured *in vivo* and related to loss of alveolar epithelial type II cells (ATII) as well as increased mesenchymal marker. *Il6* null mice exhibited preserved ATII survival, reduced myofibroblasts and improved elastic fiber assembly, thus enabling lung growth and protecting lung function. Pharmacological inhibition of global IL-6 signaling and IL-6 trans-signaling promoted alveolarization and ATII survival after hyperoxia. Third, hyperoxia triggered M1-like polarization, possibly *via* Klf4; hyperoxia-conditioned medium of macrophages and IL-6 impaired ATII proliferation. Finally, clinical data demonstrate elevated macrophage-related plasma cytokines as potential biomarkers that identify infants receiving oxygen at increased risk of developing BPD. Moreover, macrophage-derived *IL6* and active STAT3 were related to loss of epithelial cells in BPD lungs.

Conclusion: We present a novel IL-6-mediated mechanism by which hyperoxia activates macrophages in immature lungs, impairs ATII homeostasis, and disrupts elastic fiber formation, thereby inhibiting lung growth. The data provide evidence that IL-6 trans-signaling could offer an innovative pharmacological target to enable lung growth in severe neonatal chronic lung disease.

Introduction:

Premature infants often require respiratory support, including mechanical ventilation (MV) and/or supplemental oxygen. However, these life-saving treatments when applied to the immature lung can impair lung growth, leading to neonatal chronic lung disease, initially described as bronchopulmonary dysplasia (BPD) (1). Lungs of infants afflicted with BPD are typically characterized by reduced formation of alveoli and perturbed matrix remodeling, yielding structural changes that may persist beyond adolescence (2, 3). Despite significant advances in neonatal management over the past decades, the incidence of BPD remains high, with a lack of effective preventive or therapeutic strategies. Thus, identifying new molecular pathways that impair alveolar growth and regeneration after injury of the immature lung may lead to potential novel therapeutics.

Alveolar epithelial type I (ATI) and type II (ATII) cells lining the alveoli are injured when exposed to hyperoxia and this likely contributes to the pathogenesis of BPD (4, 5). Alveolar regeneration is primarily directed by ATII, which have the capacity for self-renewal and give rise to ATI after lung injury (6). Disruption of ATII homeostasis is involved in the pathogenesis of various chronic lung diseases, including BPD (7, 8). Hyperoxia reduces survival and induces epithelial mesenchymal transition (EMT) in ATII (9, 10). Growth factors and cytokines can modulate ATII homeostasis, reducing alveolar formation and regeneration (10, 11). Thus, changes in the pulmonary microenvironment after hyperoxia may complicate the course of BPD by decreasing ATII survival and alveolar growth.

The pathogenesis of BPD also includes changes in immune cell proportions, but the mechanisms and the role of distinct immune cells in BPD pathogenesis are not yet known (12, 13). Recent studies demonstrated that resident and non-resident macrophages are key constituents of the inflammatory lung environment in response to injury, orchestrating it through secretion of various cytokines, including Interleukin 6 (IL-6), a regulator of cell homeostasis, matrix remodeling, immune response and tissue regeneration (14). On the other hand, macrophages also contribute to a regenerative niche, essential for repair after lung injury (15). Anti-inflammatory approaches attenuate impaired alveolarization induced by hyperoxia (16, 17). However, the impact of oxygen on the regulation of the inflammatory lung microenvironment as well as its impact on ATII homeostasis and alveolar formation remain elusive.

In this study, we present evidence that prolonged oxygen exposure recapitulates severe neonatal chronic lung disease, activates macrophages, favoring M1-like polarization and resulting in increased IL-6 activity in newborn lungs. Of note, we demonstrate that specific blockade of IL-6 trans-signaling preserves ATII survival and enables lung growth after hyperoxia. Mechanistically, we show that the secretome of hyperoxia-exposed macrophages inhibits ATII survival, and we identify a possible novel role for the transcription factor Krüppel-like factor 4 (Klf4) in accentuating the macrophage response after hyperoxia. In human cell culture studies, we demonstrate that hyperoxia-activated pro-inflammatory M1-like macrophages have an additive effect on hyperoxia-reduced survival of human alveolar epithelial cells (hAEC). Finally, we confirmed that the macrophage-driven inflammatory IL-6/STAT3 response is present in lungs or in the serum of infants with BPD.

Material and Methods

Extended description of the material and methods is provided in the online supplement.

Animal experiments

Animals studies were divided into four groups: (i) exposure of male and female newborn mice on a C57Bl6 background to hyperoxia (80 % O_2) for 14 days for transcriptomic analysis of whole lungs, and to 40% or 85% O_2 for 3, 7 or 28 days for subsequent assessment of IL-6 signaling; (ii) exposure of newborn C57BL6 mice as well as (iii) newborn B6.129S2-*Il6*$^{tm1Kopf/J}$ (*Il6*$^{-/-}$) and their respective WT control to hyperoxia (85 % O_2) for 28 days to determine long-term effects of hyperoxia. Finally, (iv) newborn mice were treated intraperitoneally with soluble gp130Fc or IL-6 mAb at postnatal days (P) 2, P7, P14, and P21. See details and description of pulmonary function tests in the online supplement.

Tissue Assays

RNA extraction, mRNA measurement: RNA extraction and qRT-PCR were performed as previously described (18).

Transcriptomic analysis using RNA Sequencing, Bioinformatics analyses and in-silico cellular deconvolution: All statistical analyses were obtained with the R statistical framework. Pathway

analysis was performed on *Mus musculus* pathways from the KEGG database and StringDB database (19). *In silico* cellular deconvolution was performed using the immunoStates (iS) method (20).

Protein extraction and immunoblots: Protein extraction, protein measurements, and immunoblots were performed as described previously (18). Antibodies are listed in the online supplement

Postmortem processing of lungs for quantitative histology immunostaining: Septal thickness, mean linear intercept, radial alveolar count, surface of a single alveolus, insoluble lung elastin, and microvessels were assessed as described previously (21) and in detail in the online supplement. Lungs were stained for CD68 (macrophages), αSMA^+ (myofibroblasts), pro-SFTPC (ATII) and cell death (TUNEL). Positive stained cells were counted as detailed in the online supplement.

Cell Culture Studies

Cell lines, reagents, and assays: Murine lung epithelial cells (MLE-12; ATCC), macrophages (J774A.1; ATCC), primary murine macrophages (peritoneal) from wildtype mice, human monocyte-derived macrophages from donors, and human alveolar epithelial cells (hAEC, CellBiologics; PELOBiotech, Germany) were studied. For ethical consent and detailed information, please see online supplement. MLE12 and hAEC cells were exposed to mouse or human IL-6 (Sigma-Aldrich, Germany) + mouse or human IL-6Ra (IL-6Ra Protein, R&D Systems, USA) (IL-6/sIL-6R). Proliferation was assessed using MTT assay (ATCC; #30-1010K). IL-6 was measured using ELISA (IL-6 ELISA, Invitrogen, USA). Klf4 was silenced in macrophages (J774.A1) with si-klf4 (Dharmacon, Cat. No. SO-2589106G, USA) using Endo-Porter (GeneTools LLC, Philomath, USA).

Precision-Cut Lung Slices (PCLS):

Murine lungs were isolated from the 14-days old mice after intratracheal instillation of agarose. PCLS were treated with IL-6 (Sigma-Aldrich, Germany) + 20 ng IL-6Ra (IL-6Ra Protein, R&D Systems, USA) (IL-6/sIL-6R) under normoxia (21 % O_2, NOX) or hyperoxia (85 % O_2, HYX) for 48 h. Subsequently, PCLS were fixed with 4 % PFA and paraffin-embedded for immunofluorescence staining for SFTPC and TUNEL detection (*in situ* Cell Death Detection Kit, Roche, Germany).

Human lung tissue

BPD and control (non-diseased) lung tissues were obtained through the NHLBI LungMAP Consortium Human Tissue Core Biorepository (BRINDL). The Biorepository is approved by the University of Rochester Research Subjects Review Board (RSRB00056775). Consent for research use has been provided for each sample. Clinical metadata and histopathology are listed in Table 1.

Immunostaining of human lungs

BPD and control lungs were stained for pSTAT3 (1:200; Cell Signaling, #9145), CD45 (1:200; Invitrogen, 14-9457-82), CDH1 (1:200, BD Biosciences, 610181), CD68 (1:200, eBioscience, 14-0688-82), and SFTPC (1:100, LSBio, LS-B10952).

In Situ Hybridization of Human Lungs

Fluorescent in situ hybridization for *Il6* was conducted using the Advanced Cell Diagnostics RNAscope Fluorescent Multiplex Assay.

Clinical Studies

55 infants born at <32 weeks gestation were enrolled into a longitudinal cohort of patients at Lucile Packard Children's Hospital. Stanford University's Institutional Review Board approved the study. Informed parental consent was granted for each infant enrolled in the study. Infants were followed up to 36 weeks post-menstrual age. Plasma samples were assayed for cytokine profiling by 63-plex bead assay. Clinical data are summarized in supplementary table 2.

Statistical Analysis

All continuous measurements are expressed as mean ± standard error of the mean (SEM) and $p<0.05$ denoted significant differences. For *in vivo* murine studies, Two-way ANOVA or one-way ANOVA followed by a Dunn's or Bonferroni's post-test, respectively, Mann-Whitney-test, and Student's t-test were used to test for statistical significance. For cell culture studies, we applied (Repeated Measures) one-way ANOVA followed by a Bonferroni's post-test or paired t-test. For human studies, we used Mann-Whitney test, Student's t-test, non-parametric fitted curve and mixed linear model.

Results:

Transcriptomic analysis identifies chemokine signaling as the most regulated pathway in murine lungs after hyperoxia

RNAseq transcriptomic profiling was performed as depicted in Fig. 1A. Genes with average log-fold change (FC) greater than 2 and FDR-corrected p-value <0.01 were considered as differentially expressed genes (DEG) (Figure 1B, C). Pathway analysis on the KEGG pathway database identified a number of relevant pathways. Of these, the most notable were the *Cytokine-cytokine receptor interaction* and *Chemokine-mediated signaling pathway* (Figure 1D). To identify putative functional networks we used DEGs in the ten most up- and down-regulated KEGG pathways as input for StringDB (Figure 1E-H). First, we identified the ten most significant biological processes (Figure 1E) and molecular functions (Figure 1F) using gene ontology (GO) analysis. Second, based on DEGs in the ten most regulated KEGG pathways we generated a functional network (Figure 1H), which highlighted the centrality of DEGs. Each DEG in the functional network has a color-code, which allows the individual assignment to the biological processes shown in Figure 1E. We next defined a ranking for the centrality of each DEG and identified the top ten hubs. Of these hubs, nine are chemokines related to macrophage function (Figure 1G).

***In-silico* cellular deconvolution identifies inflammatory immune cell dysregulation in neonatal lungs after hyperoxia**

We next applied the immunoStates method to the gene expression data to assess if any immune cell type showed different proportions in hyperoxia compared to normoxia. Myeloid dendritic cells, naïve B cells, and plasma cells were increased; whereas $CD4^+$, $CD56^+$ and mast cells were significantly reduced. Consistent with our hypothesis, pro-inflammatory M1-like macrophages proportions were higher in the hyperoxia group. In contrast, activated, anti-inflammatory M2-like macrophages proportions were lower (Figure 2A, B). We confirmed these findings using qRT-PCR to determine the expression of key macrophage-regulating markers (*Ccl7, Cxcl5*, and *Ccl2*) (Figure 2C). Furthermore, hyperoxia increased additional targets in lungs of newborn mice that are genes observed in M1-like polarization encoding *Il6*, *Il17A*, and *Mmp12* (Figure 2D). In contrast, M2-like markers, e.g. *Il4*, *Il13*, *Arg1*, were not significantly different between the two groups (Figure 2E). To assess gene expression and the effect of oxygen concentration at earlier developmental time points we performed qRT-PCR

on M1- and M2-like markers at P3 and P7 in lungs of mice exposed either to 40% or 85% O_2. The gene expression analyses revealed a marked lung-intrinsic increase in *Il6* and *Mmp12* (M1-like markers), whereas the M2-like markers (*Il4* and *Arg1*) were reduced at P3 and P7 after 85 % O_2 (Supplementary Figure 1A-D).

IL-6/STAT3 signaling in neonatal mouse lungs after hyperoxia is related to loss of epithelial cells and increased mesenchymal markers.

Since *Il6* mRNA was almost 20-fold upregulated in lungs of newborn mice exposed to prolonged hyperoxia (85 % O_2), we assessed lung IL-6/STAT3 signaling early after birth (P3, P7) and at P28. At P3 and P7, the significant increase of IL-6 mRNA was related to a marked activation of its downstream effector, STAT3, and expression of its target gene *Socs3* at P7. Exposure to lower concentrations of oxygen (40 % O_2) induced phosphorylation of STAT3 (p=0.0556) and a significant expression of Socs3 at P3 (Supplementary Figure 2). In order to investigate severe chronic lung injury after oxygen we continued the experiments with 85 % O_2. At P28, we found 5-fold increased IL-6 protein, a significant activation of its downstream effector, STAT3, and a higher expression of SOCS3 after hyperoxia when compared to normoxia (Figure 2F-H and Supplementary Figure 3). These pro-inflammatory findings were related to an almost 5-fold increased expression of αsma, also known as *Acta2*, a mesenchymal marker expressed by smooth muscle cells and myofibroblasts (Figure 2I), and a lower protein abundance of surfactant protein C (SFTPC) and aquaporin 5 (AQP5), ATII and ATI markers, respectively (Figure 2J, K).

Loss of IL-6 preserves alveolar formation in newborn mice after hyperoxia

We next tested if loss of *Il6* would protect the newborn mice from hyperoxia-induced lung injury and permit alveolar formation. Although hyperoxia simplified alveoli in the WT mice as indicated by reduced radial alveolar count (RAC) and increased mean linear intercept (MLI), these abnormalities were attenuated in the $Il6^{-/-}$ mice (Figure 3A-C). Similarly, *Il6* deficiency protected newborn mice from the 50 % increase of the alveolar surface area of single alveoli observed in WT mice, reflecting an ability to develop a greater overall gas exchange surface area (Figure 3D).

Loss of IL-6 preserves elastic fiber assembly and lung compliance after hyperoxia

Hyperoxia disrupted elastin deposition in WT lungs, leading to a loss of elastin at the tips of the secondary septae and "brush-like" elastic fibers in the primary septae (Figure 3E). In contrast, less disorganized elastic fibers were detected in the lungs of hyperoxia-exposed *Il6*$^{-/-}$ mice, and the localization at the tips of the secondary septae appeared similar to that observed in the normoxia-exposed animals. The absolute elastic fiber content per defined area (μm^2) was unaltered by hyperoxia or IL-6 deficiency. Hyperoxia, however, significantly increased the relative elastic fiber content in WT but not *Il6*$^{-/-}$ mice (Figure 3F, G). These changes in elastic fiber localization may account for the protection of *Il6*$^{-/-}$ from reduced lung compliance after hyperoxia (Figure 3H). We next analyzed elastic fiber components and found an increase in *Col1a1*, *Fbn1*, and *Fbln5* mRNA in *Il6*$^{-/-}$ lungs compared to WT (Figure 3I-K). Moreover, deficiency of *Il6* was associated with a decrease in myofibroblasts in both normoxia and hyperoxia (Figure 3L, M). Although hyperoxia induced macrophage influx in both WT and *Il6*$^{-/-}$ mice, macrophage abundance was significantly lower in the hyperoxia-exposed *Il6*$^{-/-}$ mice than in WT (Figure 3N, O).

Loss of IL-6 promotes surfactant protein expression and protects ATII after hyperoxia

Hyperoxia reduced *Sftpa* and *Sftpc* mRNA by almost 50 % in WT mice, an effect that was completely blocked in the *Il6*$^{-/-}$ mice (Figure 4A, B). In keeping with this finding, the protein abundance of SFTPC was significantly higher in hyperoxia-exposed *Il6*$^{-/-}$ mice compared to WT (Figure 4C). Using immunofluorescent staining for SFTPC, we demonstrate that hyperoxia decreased the number of $SFTPC^+$ cells in both groups; however, $SFTPC^+$ cells were significantly higher in hyperoxia-exposed *Il6*$^{-/-}$ as compared to WT (Figure 4D, E). Finally, using TUNEL staining we found that cell death, including ATII, was approximately 50 % lower in the hyperoxia-exposed *Il6*$^{-/-}$ mice when compared to WT (Figure 4F-H).

Pharmacological inhibition of global IL-6 signaling and IL-6 trans-signaling

We next treated newborn mice weekly, while exposed to hyperoxia, with injections of either IL-6 mAb sgp130Fc, or the respective vehicle (22) (Fig. 5A). While IL-6mAb globally neutralizes IL-6, sgp130Fc only blocks the complex formed by IL-6 and sIL-6 receptor, which is called IL-6 trans-

signaling. Hyperoxia reduced survival of the newborn mice by ~20%, but treatment with IL-6 mAb or sgp130FC protected the mice (Fig. 5B). Both IL-6 mAb and sgp130Fc preserved alveolarization in lungs exposed to prolonged hyperoxia (Fig. 5C-F), indicating that IL-6 trans-signaling *via* the soluble IL-6 receptor was in part the underlying mechanism. Moreover, we found that mice treated with IL-6 mAb or sgp130Fc under hyperoxia were protected from loss of ATII, and had a similar number of ATII when compared to vehicle-treated mice under normoxia (Fig. 5G, H).

Hyperoxia activates macrophages *via* loss of Klf4 and hyperoxia-exposed macrophages reduce cell survival of ATII

Hyperoxia lowered the gene expression of the epithelial cell markers *Sftpc*, but not *Aqp5* in lung epithelial cells (MLE12) as indicators of ATII and ATI, respectively. Treatment of MLE12 with IL-6/sIL-6R had an additive effect on the reduction of *Sftpc*, but not *Aqp5* (Figure 6A). To determine whether the secretome of macrophages (J774A1) regulates cell survival of MLE12, we exposed MLE12 cells to hyperoxia, followed by treatment with either standard cell medium (Co), normoxia-conditioned macrophage medium (CM^{NOX}) or hyperoxia-conditioned macrophage medium (CM^{HYX}). While the effect of CM^{NOX} was similar to CM^{Co}, CM^{HYX} reduced proliferation of MLE12 (Figure 6B). We next found that exposing macrophages (J774A.1) to hyperoxia for 24 and 48 h *in vitro*, significantly increased IL-6 protein in the conditioned medium (Figure 6C). In addition, we studied a possible mechanism by which hyperoxia activates M1-like polarization. Prior reports have shown that loss of Klf4 promotes M1-like polarization (23). Indeed, hyperoxia reduced Klf4 protein in cultured macrophages by more than 50 % (Figure 6D). Furthermore, silencing of Klf4 in macrophages accentuated the expression of pro-inflammatory (M1-like) cytokines induced by hyperoxia (Figure 6E). We next exposed primary murine macrophages (peritoneal) from WT mice to hyperoxia and found a significantly increased expression of *Mmp12* and *Tlr4* (M1-like) and a marked reduction of *Arg1* and *Fizz1* (M2-like) (Figure 6F). Moreover, CM^{HYX} further decreased cell proliferation of MLE12 under hyperoxia when compared to CM^{NOX} (Figure 6G). Finally, we exposed PCLS of 14-days old mice to IL-6/sIL-6R to normoxia or hyperoxia. IL-6 caused apoptosis in PCLS and had a significant additive effect on hyperoxia-induced apoptosis of $SFTPC^{+}$ cells (ATII) (Figure 6 H).

To translate our data to humans we used human AEC (hAEC, see Supplementary Figure 4) and human monocyte-derived macrophages. Treatment of hAEC with IL-6/sIL-6R significantly reduced

proliferation under normoxia and hyperoxia for 24 h (Figure 7A). We next exposed hAEC to standard cell medium (Co), to normoxia-conditioned human M1-like macrophage medium (hCM^{NOX}) or to hyperoxia-conditioned medium of human M1-like macrophages (hCM^{HYX}). Similar to the murine studies, we found that hCM^{HYX}, but not hCM^{NOX} further decreased proliferation of hAEC (Figure 7B). Interestingly, CM^{HYX} of M0-like macrophages did not have an additive effect on hyperoxia-reduced proliferation of hAEC when compared to CM^{NOX} (Supplementary Figure 5). Finally, exposure of M1-like differentiated human monocyte-derived macrophages to hyperoxia for 48 h increased significantly the gene expression of human *IL6* (h*IL6*), *TNFa*, *TLR4*, and *IL1b* (Figure 7B).

Inflammatory serum biomarker profiling in premature infants for oxygen and BPD

Cytokine multiplex assay in plasma of preterm infants determined macrophage-related cytokines (RANTES, MCP3, MIG) and IL-6 (Figure 8A) as potential biomarkers that identify infants receiving oxygen therapy at risk of developing BPD. By mixed linear modelling, infants that progressed to BPD demonstrated a longitudinal pattern of changes in plasma cytokine levels that differed from that seen in infants that did not develop BPD (Figure 8B-E). Moreover, we performed a nonparametric fitted curve, followed by statistical analysis to determine the difference between BPD vs non-BPD at 32 weeks and 36 weeks (Figure 8F). We found at 32 weeks in infants developing BPD increased concentrations of IL1RA ($p=0.025$), and a trend for increased ICAM (CD54; $p=0.075$). These cytokines are either polarizing or secreted by macrophages. At 36 weeks, we only detected a mild but not significant elevation of IFNG ($p=0.16$), and MIP1A (CCL3; $p=0.15$), likely owing to small sample size. This will need to be verified through larger prospective longitudinal studies.

Immune ($CD45^+$ and $CD68^+$) cell influx with activation of IL-6/STAT3 signaling and reduced epithelial cells in lungs of infants with BPD

Finally, we analyzed six postnatal human BPD lungs and six age-matched control lungs (Table 1). CD45 immunofluorescent staining displayed a significant increase of immune cells in BPD lungs. Subsequent specific staining for CD45 and CD68, a marker of macrophages, showed significantly higher number of immune cells and macrophages in lungs with BPD when compared to non-BPD (Figure 9A, B). *In situ* hybridization of h*IL6* revealed higher number of h*IL6* mRNA-expressing cells in lungs with BPD when compared to the age-matched control lungs (Figure 9C). The combination of

in situ hybridization of h*IL6* and CD68 immunofluorescent staining demonstrated significantly higher expression of h*IL6* in macrophages in lungs with BPD than in non-BPD (Figure 9D). Immunofluorescent staining for STAT3 as downstream of IL-6, and CHD1 (epithelial cell marker) showed an activation of STAT3 and a reduction of $CDH1^+$ cells only in sex- and age-matched pairs (male), whereas infants matching for age, but not for sex (male vs. female) did not show significant changes, indicating possible sex-specific differences (Figure 9E-H). Finally, we stained for SFTPC as a marker of ATII and found an age-related association of number of ATII with BPD. The age of the infants with BPD significantly correlated with the decrease of ATII (R^2=0.5794; p = 0.0062), whereas non-BPD showed a trend of increased ATII with age (Figure 9I). In summary, these data demonstrate that the pathogenesis of BPD is intimately linked to inflammation with macrophage-derived h*IL6*, STAT3 activation, and ultimately loss of epithelial cells and ATII over time.

Discussion

This study presents a novel mechanism by which hyperoxia adversely affects ATII homeostasis and elastic fiber formation *via* macrophage activation, resulting in enhanced activation of the IL-6 axis by IL-6 trans-signaling *via* soluble IL-6 receptor, and ultimately inhibiting alveolar formation and impairing lung function. The data provide strong evidence that inhibition of IL-6-trans-signaling offers an innovative pharmacological target to enable lung growth in premature infants at risk for BPD. This novel inflammatory paradigm in the pathogenesis of BPD is based on *in vivo* studies using genetic modified mice with deletion of *Il6*, pharmacological treatment targeting global and IL-6 trans-signaling, and finally human studies using serum and lungs of infants with and without BPD along with human AEC and monocyte-derived macrophage cell culture studies.

Inflammation is a central mechanism in BPD (13). Recent studies highlighted that resident alveolar macrophages are activated by hyperoxia, causing them to contribute to abnormal structural development of the immature mouse lung (15). Kalymbetova and colleagues show that hyperoxia causes a loss of resident alveolar macrophages in lungs of newborn mice, while a novel population of $CD45^+CD11c^+SiglecF^+CD11b^+CD68^+MHCII^+$cells emerges. The authors propose that residential alveolar macrophages transdifferentiate into this new population that contributes to arrested alveolarization (15). In the present study, we applied for the first time, a comprehensive bioinformatics approach using *in silico* deconvolution of cell proportions from transcriptomic data in

an experimental BPD model. We determined an immune cell proportion with reduction of the T-cell and increase in the B-cell population in lungs of mice exposed to prolonged hyperoxia. This is similar to a recent report showing a significant depletion of single positive $CD4^+$ as well as $CD8^+$ T cells (24), and an increased proportion of naïve B-cells after hyperoxia (25). Most striking, our data identified a reduction of M2-like macrophages, and an upregulation of M1-like macrophages that could possibly emerge from resident alveolar macrophages (15). To further test this notion and to define the diverse macrophage phenotypes scRNASeq over time should be performed.

Further analyses verified that chemokines regulating macrophage function are highly upregulated by hyperoxia, and that cytokine-cytokine receptor interaction and IL-17 signaling are the most affected pathways. Interestingly, IL-6 directs the immune response toward the Th17 phenotype, and IL-17 increases after hyperoxia in both alveolar macrophages and in lung epithelial cells (26, 27). The role of IL-6 in neonatal lung injury, however, has been controversially discussed. While overexpression of IL-6 aggravated lung injury in newborn mice that were exposed to hyperoxia after birth, IL-6 overexpression provides protective effects against oxidant-mediated injury when mice are exposed to hyperoxia from day 3 to 6 of life (28, 29). In contrast, the present study demonstrates that *Il6* null mice exhibit a mild reduction of alveoli already under normoxia that could be related to reduced number of myofibroblasts and possibly impaired secondary septation. While this notion is speculative and requires further investigation, our current findings along with prior studies highlight the importance of the tight regulation of IL-6 during discrete windows of lung development.

Various experimental models have been used to investigate the pathogenesis of BPD, including exposure to increased concentrations of oxygen, mechanical ventilation or infection (10, 30, 31). When interpreting data, various criteria including sex, age, strain, injurious stimuli, and duration of exposure have to be taken into account (32-34). Reports demonstrated that the injury and the lung phenotype depend on the injurious stimuli and on the time of exposure. For example, continuous exposure to 40 % O_2 from P1 until P4 or P14 adversely impacted alveolar formation and gas exchange surface, but not septal wall thickness as an indicator of matrix remodeling. On the contrary, only the severe BPD model with exposure of newborn mouse pups to 85 % O_2 recapitulated both a marked impact on alveolarization and on alveolar septal wall thickness that is often seen in human disease (32, 35, 36). In the present study, we used 85 % O_2 for a prolonged period to induce a severe chronic

lung injury with marked inflammation. Future studies, however, should include the impact of oxygen concentration and time of exposure in combination with mechanical ventilation and/or infection.

IL-6 is a multifunctional pro-inflammatory cytokine that regulates cell survival, differentiation of immune cells, such as macrophages, neutrophils as well as T-cells, and induces matrix remodeling that favors fibrosis (37, 38) as seen in chronic lung diseases (39). Clinical studies showed increased concentrations of IL-6, sIL-6R, and sgp130 in tracheal aspirates of infants evolving BPD (40-42). ATII-macrophage interaction has been suggested by prior studies showing that alveolar epithelial IL-6-activated STAT3 signaling mediates inflammation, likely *via* macrophages (43). We provide evidence *in vivo* and *in vitro* that hyperoxia disrupts macrophage-hAEC interaction by increasing various macrophage regulating cytokines, including *Il6*, inducing cell death of hAEC and promoting M1-like differentiation of macrophages (44, 45). Since a previous study showed that the reduction of Klf4 favors M1-like polarization, our present findings might be possibly related to a loss of Klf4 after hyperoxia (23). Collectively, our data highlight the degree to which hyperoxia dysregulates the alveolar epithelial-macrophage niche, but also the key role of IL-6 in orchestrating this cellular crosstalk. Recent reports suggest that targeting IL-6 signaling prevents emphysema-like disease (46), and may be a new therapeutic target for pulmonary arterial hypertension (47). Here, we provide evidence that loss of IL-6 and pharmacological inhibition of IL-6 classic- and trans-signaling enables alveolar growth and lung function by protecting ATII survival and preserving distribution of elastic fibers in lungs of newborn mice after hyperoxia. Recent studies indicated that inhibition of proteolytic activity in mechanically-ventilated newborn mice using the serine elastase inhibitor elafin enabled lung growth and reduced inflammation (21, 30). The key role of protease and anti-protease balance in neonatal lung growth was further supported by the finding that infants evolving BPD have increased serum elastase concentrations (30). Interestingly, proteases (e.g., ADAM10 or ADAM17) have been described to act as a sheddase for the IL-6 receptor and a regulator of IL-6 signaling (48-50). Thus, blocking of proteolytic activity could have an anti-inflammatory effect by preventing IL-6 signaling.

Inflammatory response and dysregulation of cytokines is a prominent feature of BPD. Increased number of immune cells in BPD is associated with decreased septation and fewer alveoli (12, 13, 15). In the present study, we determined increased concentrations of plasma cytokines regulating macrophage recruitment and function, such as RANTES, MCP3, and MIG3, highlighting

the systemic inflammatory response in BPD. Similarly, we found a marked upregulation of IL1RA and ICAM1, both cytokines regulating macrophage polarization (51, 52). Interestingly, serum ICAM level has been recently reported as a potential biomarker for BPD and was correlated with its severity (53). Plasma IL-6 concentration was dynamically regulated with an early postnatal elevation of IL-6 by trend in infants developing BPD when compared to non-BPD. Since Plasma does not necessarily reflect lung-intrinsic IL-6, tracheal aspirates might be more appropriate as shown in prior studies with increased IL-6 in infants with BPD (42). However, the time point of measurement in the infant might not developmentally match our mouse model. The plasma cytokine pattern in infants with BPD was related to a significant increase of immune cells, specifically macrophages ($CD68^+$), and increased macrophage-derived *Il6* in lungs of infants with BPD, independent of sex and age. We linked this immune response to an activation of STAT3 signaling and loss of epithelial cells in male infants. Interestingly, these effects were not evident in age-matched, but not sex-matched BPD and non-BPD infants, suggesting a possible sex-specific IL-6/STAT3 response, which could contribute to sex-dependent differences in BPD (54). Finally, we showed a correlation between age and the reduction of ATII in lungs with BPD, but not in non-BPD. Taken together our studies, in concert with prior studies, suggest that IL-6 as a macrophage-regulating cytokine, might serve as a useful biomarker of lung injury in very premature infants, and help to define the risk for BPD.

As depicted in our working model (Figure 10A, B), inflammation and damage of the regenerative epithelial niche by loss of ATII impairs alveolar formation and leads to emphysematous lung structure beyond infancy. The present study demonstrates that hyperoxia disrupts macrophage-ATII interaction by triggering IL-6/STAT3 signaling in murine and human lungs, but also identifies IL-6 as a potential early-onset biomarker and sgp130Fc as a novel therapeutic strategy for infants at risk for BPD. The specific blockade of IL-6 trans-signaling predominantly inhibits the pro-inflammatory activities of IL-6 while the protective and regenerative function is not affected. This innovative therapeutic strategy is already in phase II clinical trial in patients with autoimmune disease (55) and offers new avenues for the treatment of BPD.

Acknowledgements

We greatly appreciate and thank Prof. Marlene Rabinovitch and Prof. Richard Bland (Departments of Pediatrics, Departments of Cardiovascular Institute, and The Vera Moulton Wall Center for Pulmonary Vascular Disease, Stanford University School of Medicine, Stanford) for their helpful suggestions. We thank the imaging facility of the Cologne Excellence Cluster on Cellular Stress Responses in Aging-Associated Diseases (CECAD) for their technical support. We also thank Dr. Sebahattin Cirak (Department of Pediatrics, Center for Molecular Medicine Cologne, and Center for Rare Diseases Cologne, University of Cologne, University Hospital of Cologne, Cologne, Germany), and Dr. Ugur Akpulat (Department of Pediatrics, Center for Molecular Medicine Cologne, University of Cologne, University Hospital of Cologne, Cologne, Germany; and University of Kastamonu, Turkey) for their technical support in cell culture studies. The IL-6mAb and sgp130Fc was kindly provided by Prof. Dr. Stefan Rose-John (Institute of Biochemistry, Christian-Albrechts-University Kiel, Germany).

Funding sources

This work was supported by Deutsche Forschungsgemeinschaft [1636/2-1; MAAA], Marga und Walter Boll Stiftung (MAAA); Center for Molecular Medicine Cologne (CMMC; MAAA), and University Hospital Cologne; Stanford Child Health Research Institute Tashia and John Morgridge Faculty Scholar Award (CMA); the NIH HL122918 (CMA), NIH R01HL141856 (DA), NIH PO1HL108797-5974 Biomarker Core (CM); NHLBI LungMAP Research Center. U01HL122681 (SD, DA), Biorepository (1U01HL122700, GP) and Data Coordinating Center (1U01HL122638, GP).

Author Contributions

D.H, C.M.A., S.D., C.M., D.A., V.B., C.P., S.R.J, M.O., G.S.P., R.S., and M.A.A.A. conceived and designed research; D.H., C.M.A., S.D., M.D., C.M., K.D., C.V., J.M., V.B., S.M., and M.A.A.A. performed experiments; D.H., C.M.A., S.D., M.D., C.M., L.T., C.V., D.A., and M.A.A.A. analyzed data; D.H., C.M.A., S.D., M.D., C.M., L.T., J.S., S.v.K.R., J.M., P.K. D.A., J.D., and M.A.A.A. interpreted results of experiments; D.H., S.D., M.D., J.S., and M.A.A.A. prepared figures; D.H., and M.A.A.A. drafted manuscript; D.H., C.M.A., S.D., C.M., D.A., J.S., W.S., and M.A.A.A. edited and revised manuscript. D.H., C.M.A., S.D., M.D., C.M., L.T., J.M., K.D., C.V., J.S., S.v.K.R., V.B., C.P., S.R.J., M.O., G.S.P., R.S., S. M., W.S., P.K. D.A., J.D., and M.A.A.A. approved final version of manuscript.

References:

1. Northway WH, Jr., Rosan RC, Porter DY. Pulmonary disease following respirator therapy of hyaline-membrane disease. Bronchopulmonary dysplasia. *N Engl J Med* 1967; 276: 357-368.
2. Caskey S, Gough A, Rowan S, Gillespie S, Clarke J, Riley M, Megarry J, Nicholls P, Patterson C, Halliday HL, Shields MD, McGarvey L. Structural and Functional Lung Impairment in Adult Survivors of Bronchopulmonary Dysplasia. *Ann Am Thorac Soc* 2016; 13: 1262-1270.
3. Thebaud B, Abman SH. Bronchopulmonary dysplasia: where have all the vessels gone? Roles of angiogenic growth factors in chronic lung disease. *Am J Respir Crit Care Med* 2007; 175: 978-985.
4. Hou A, Fu J, Yang H, Zhu Y, Pan Y, Xu S, Xue X. Hyperoxia stimulates the transdifferentiation of type II alveolar epithelial cells in newborn rats. *Am J Physiol Lung Cell Mol Physiol* 2015; 308: L861-872.
5. Yee M, Buczynski BW, O'Reilly MA. Neonatal hyperoxia stimulates the expansion of alveolar epithelial type II cells. *Am J Respir Cell Mol Biol* 2014; 50: 757-766.
6. Rackley CR, Stripp BR. Building and maintaining the epithelium of the lung. *J Clin Invest* 2012; 122: 2724-2730.
7. Vaughan AE, Chapman HA. Failure of Alveolar Type 2 Cell Maintenance Links Neonatal Distress with Adult Lung Disease. *Am J Respir Cell Mol Biol* 2017; 56: 415-416.
8. Yee M, Domm W, Gelein R, Bentley KL, Kottmann RM, Sime PJ, Lawrence BP, O'Reilly MA. Alternative Progenitor Lineages Regenerate the Adult Lung Depleted of Alveolar Epithelial Type 2 Cells. *Am J Respir Cell Mol Biol* 2017; 56: 453-464.
9. Vyas-Read S, Wang W, Kato S, Colvocoresses-Dodds J, Fifadara NH, Gauthier TW, Helms MN, Carlton DP, Brown LA. Hyperoxia induces alveolar epithelial-to-mesenchymal cell transition. *Am J Physiol Lung Cell Mol Physiol* 2014; 306: L326-340.
10. Alejandre-Alcazar MA, Kwapiszewska G, Reiss I, Amarie OV, Marsh LM, Sevilla-Perez J, Wygrecka M, Eul B, Kobrich S, Hesse M, Schermuly RT, Seeger W, Eickelberg O, Morty RE. Hyperoxia modulates TGF-beta/BMP signaling in a mouse model of bronchopulmonary dysplasia. *Am J Physiol Lung Cell Mol Physiol* 2007; 292: L537-549.
11. Maloney JP, Gao L. Proinflammatory Cytokines Increase Vascular Endothelial Growth Factor Expression in Alveolar Epithelial Cells. *Mediators Inflamm* 2015; 2015: 387842.
12. Bhandari V, Choo-Wing R, Lee CG, Zhu Z, Nedrelow JH, Chupp GL, Zhang X, Matthay MA, Ware LB, Homer RJ, Lee PJ, Geick A, de Fougerolles AR, Elias JA. Hyperoxia causes angiopoietin 2-mediated acute lung injury and necrotic cell death. *Nat Med* 2006; 12: 1286-1293.
13. Liao J, Kapadia VS, Brown LS, Cheong N, Longoria C, Mija D, Ramgopal M, Mirpuri J, McCurnin DC, Savani RC. The NLRP3 inflammasome is critically involved in the development of bronchopulmonary dysplasia. *Nat Commun* 2015; 6: 8977.
14. Wolf J, Rose-John S, Garbers C. Interleukin-6 and its receptors: a highly regulated and dynamic system. *Cytokine* 2014; 70: 11-20.
15. Kalymbetova TV, Selvakumar B, Rodriguez-Castillo JA, Gunjak M, Malainou C, Heindl MR, Moiseenko A, Chao CM, Vadasz I, Mayer K, Lohmeyer J, Bellusci S, Bottcher-Friebertshauser E, Seeger W, Herold S, Morty RE. Resident alveolar macrophages are master regulators of arrested alveolarization in experimental bronchopulmonary dysplasia. *J Pathol* 2018; 245: 153-159.
16. Nold MF, Mangan NE, Rudloff I, Cho SX, Shariatian N, Samarasinghe TD, Skuza EM, Pedersen J, Veldman A, Berger PJ, Nold-Petry CA. Interleukin-1 receptor antagonist prevents murine bronchopulmonary dysplasia induced by perinatal inflammation and hyperoxia. *Proc Natl Acad Sci U S A* 2013; 110: 14384-14389.
17. Rudloff I, Cho SX, Bui CB, McLean C, Veldman A, Berger PJ, Nold MF, Nold-Petry CA. Refining anti-inflammatory therapy strategies for bronchopulmonary dysplasia. *J Cell Mol Med* 2017; 21: 1128-1138.
18. Mohr J, Voggel J, Vohlen C, Dinger K, Dafinger C, Fink G, Gobel H, Liebau MC, Dotsch J, Alejandre Alcazar MA. IL-6/Smad2 signaling mediates acute kidney injury and regeneration in a murine model of neonatal hyperoxia. *FASEB J* 2019: fj201801875RR.
19. Szklarczyk D, Gable AL, Lyon D, Junge A, Wyder S, Huerta-Cepas J, Simonovic M, Doncheva NT, Morris JH, Bork P, Jensen LJ, Mering CV. STRING v11: protein-protein association networks with increased coverage, supporting functional discovery in genome-wide experimental datasets. *Nucleic Acids Res* 2019; 47: D607-D613.
20. Vallania F, Tam A, Lofgren S, Schaffert S, Azad TD, Bongen E, Haynes W, Alsup M, Alonso M, Davis M, Engleman E, Khatri P. Leveraging heterogeneity across multiple datasets increases cell-mixture deconvolution accuracy and reduces biological and technical biases. *Nat Commun* 2018; 9: 4735.
21. Hilgendorff A, Parai K, Ertsey R, Jain N, Navarro EF, Peterson JL, Tamosiuniene R, Nicolls MR, Starcher BC, Rabinovitch M, Bland RD. Inhibiting lung elastase activity enables lung growth in mechanically ventilated newborn mice. *Am J Respir Crit Care Med* 2011; 184: 537-546.

22. Ruwanpura SM, McLeod L, Dousha LF, Seow HJ, Alhayyani S, Tate MD, Deswaerte V, Brooks GD, Bozinovski S, MacDonald M, Garbers C, King PT, Bardin PG, Vlahos R, Rose-John S, Anderson GP, Jenkins BJ. Therapeutic Targeting of the IL-6 Trans-Signaling/Mechanistic Target of Rapamycin Complex 1 Axis in Pulmonary Emphysema. *Am J Respir Crit Care Med* 2016; 194: 1494-1505.
23. Liao X, Sharma N, Kapadia F, Zhou G, Lu Y, Hong H, Paruchuri K, Mahabeleshwar GH, Dalmas E, Venteclef N, Flask CA, Kim J, Doreian BW, Lu KQ, Kaestner KH, Hamik A, Clement K, Jain MK. Kruppel-like factor 4 regulates macrophage polarization. *J Clin Invest* 2011; 121: 2736-2749.
24. Angusamy S, Mansour T, Abdulmageed M, Han R, Schutte BC, LaPres J, Harkema JR, Omar SA. Altered thymocyte and T cell development in neonatal mice with hyperoxia-induced lung injury. *J Perinat Med* 2018; 46: 441-449.
25. Wang J, Chen Q, Corne J, Zhu Z, Lee CG, Bhandari V, Homer RJ, Elias JA. Pulmonary expression of leukemia inhibitory factor induces B cell hyperplasia and confers protection in hyperoxia. *J Biol Chem* 2003; 278: 31226-31232.
26. Nagato AC, Bezerra FS, Talvani A, Aarestrup BJ, Aarestrup FM. Hyperoxia promotes polarization of the immune response in ovalbumin-induced airway inflammation, leading to a TH17 cell phenotype. *Immun Inflamm Dis* 2015; 3: 321-337.
27. Varelias A, Gartlan KH, Kreijveld E, Olver SD, Lor M, Kuns RD, Lineburg KE, Teal BE, Raffelt NC, Cheong M, Alexander KA, Koyama M, Markey KA, Sturgeon E, Leach J, Reddy P, Kennedy GA, Yanik GA, Blazar BR, Tey SK, Clouston AD, MacDonald KP, Cooke KR, Hill GR. Lung parenchyma-derived IL-6 promotes IL-17A-dependent acute lung injury after allogeneic stem cell transplantation. *Blood* 2015; 125: 2435-2444.
28. Choo-Wing R, Nedrelow JH, Homer RJ, Elias JA, Bhandari V. Developmental differences in the responses of IL-6 and IL-13 transgenic mice exposed to hyperoxia. *Am J Physiol Lung Cell Mol Physiol* 2007; 293: L142-150.
29. Chetty A, Cao GJ, Manzo N, Nielsen HC, Waxman A. The role of IL-6 and IL-11 in hyperoxic injury in developing lung. *Pediatr Pulmonol* 2008; 43: 297-304.
30. Alejandre Alcazar MA, Kaschwich M, Ertsey R, Preuss S, Milla C, Mujahid S, Masumi J, Khan S, Mokres LM, Tian L, Mohr J, Hirani DV, Rabinovitch M, Bland RD. Elafin treatment rescues EGFR-Klf4 signaling and lung cell survival in ventilated newborn mice. *Am J Respir Cell Mol Biol* 2018.
31. Shrestha AK, Bettini ML, Menon RT, Gopal VYN, Huang S, Edwards DP, Pammi M, Barrios R, Shivanna B. Consequences of early postnatal lipopolysaccharide exposure on developing lungs in mice. *Am J Physiol Lung Cell Mol Physiol* 2019; 316: L229-L244.
32. Leary S, Das P, Ponnalagu D, Singh H, Bhandari V. Genetic Strain and Sex Differences in a Hyperoxia-Induced Mouse Model of Varying Severity of Bronchopulmonary Dysplasia. *Am J Pathol* 2019; 189: 999-1014.
33. Tiono J, Surate Solaligue DE, Mizikova I, Nardiello C, Vadasz I, Bottcher-Friebertshauser E, Ehrhardt H, Herold S, Seeger W, Morty RE. Mouse genetic background impacts susceptibility to hyperoxia-driven perturbations to lung maturation. *Pediatr Pulmonol* 2019; 54: 1060-1077.
34. Will JP, Hirani DV, Thielen F, Klein F, Vohlen C, Dinger K, Dotsch J, Alejandre-Alcazar MA. Strain-dependent effects on lung structure, matrix remodeling and Stat3/Smad2 signaling in C57BL/6N and C57BL/6J mice after neonatal hyperoxia. *Am J Physiol Regul Integr Comp Physiol* 2019.
35. Nardiello C, Mizikova I, Silva DM, Ruiz-Camp J, Mayer K, Vadasz I, Herold S, Seeger W, Morty RE. Standardisation of oxygen exposure in the development of mouse models for bronchopulmonary dysplasia. *Dis Model Mech* 2017; 10: 185-196.
36. Yee M, Chess PR, McGrath-Morrow SA, Wang Z, Gelein R, Zhou R, Dean DA, Notter RH, O'Reilly MA. Neonatal oxygen adversely affects lung function in adult mice without altering surfactant composition or activity. *Am J Physiol Lung Cell Mol Physiol* 2009; 297: L641-649.
37. Fielding CA, Jones GW, McLoughlin RM, McLeod L, Hammond VJ, Uceda J, Williams AS, Lambie M, Foster TL, Liao CT, Rice CM, Greenhill CJ, Colmont CS, Hams E, Coles B, Kift-Morgan A, Newton Z, Craig KJ, Williams JD, Williams GT, Davies SJ, Humphreys IR, O'Donnell VB, Taylor PR, Jenkins BJ, Topley N, Jones SA. Interleukin-6 signaling drives fibrosis in unresolved inflammation. *Immunity* 2014; 40: 40-50.
38. Le TT, Karmouty-Quintana H, Melicoff E, Le TT, Weng T, Chen NY, Pedroza M, Zhou Y, Davies J, Philip K, Molina J, Luo F, George AT, Garcia-Morales LJ, Bunge RR, Bruckner BA, Loebe M, Seethamraju H, Agarwal SK, Blackburn MR. Blockade of IL-6 Trans signaling attenuates pulmonary fibrosis. *J Immunol* 2014; 193: 3755-3768.
39. Papiris SA, Tomos IP, Karakatsani A, Spathis A, Korbila I, Analitis A, Kolilekas L, Kagouridis K, Loukides S, Karakitsos P, Manali ED. High levels of IL-6 and IL-8 characterize early-on idiopathic pulmonary fibrosis acute exacerbations. *Cytokine* 2018; 102: 168-172.
40. Chakraborty M, McGreal EP, Davies PL, Nowell MA, Jones S, Kotecha S. Role of interleukin-6, its receptor and soluble gp130 in chronic lung disease of prematurity. *Neonatology* 2013; 104: 161-167.
41. von Bismarck P, Claass A, Schickor C, Krause MF, Rose-John S. Altered pulmonary interleukin-6 signaling in preterm infants developing bronchopulmonary dysplasia. *Exp Lung Res* 2008; 34: 694-706.

42. Hsiao CC, Chang JC, Tsao LY, Yang RC, Chen HN, Lee CH, Lin CY, Tsai YG. Correlates of Elevated Interleukin-6 and 8-Hydroxy-2'-Deoxyguanosine Levels in Tracheal Aspirates from Very Low Birth Weight Infants Who Develop Bronchopulmonary Dysplasia. *Pediatr Neonatol* 2017; 58: 63-69.
43. Quinton LJ, Jones MR, Robson BE, Simms BT, Whitsett JA, Mizgerd JP. Alveolar epithelial STAT3, IL-6 family cytokines, and host defense during Escherichia coli pneumonia. *Am J Respir Cell Mol Biol* 2008; 38: 699-706.
44. Chuquimia OD, Petursdottir DH, Periolo N, Fernandez C. Alveolar epithelial cells are critical in protection of the respiratory tract by secretion of factors able to modulate the activity of pulmonary macrophages and directly control bacterial growth. *Infect Immun* 2013; 81: 381-389.
45. Thorley AJ, Ford PA, Giembycz MA, Goldstraw P, Young A, Tetley TD. Differential regulation of cytokine release and leukocyte migration by lipopolysaccharide-stimulated primary human lung alveolar type II epithelial cells and macrophages. *J Immunol* 2007; 178: 463-473.
46. Petrache I, Serban K. Lost in Trans-IL-6 Signaling: Alveolar Type II Cell Death in Emphysema. *Am J Respir Crit Care Med* 2016; 194: 1441-1443.
47. Pullamsetti SS, Seeger W, Savai R. Classical IL-6 signaling: a promising therapeutic target for pulmonary arterial hypertension. *J Clin Invest* 2018; 128: 1720-1723.
48. Schumacher N, Meyer D, Mauermann A, von der Heyde J, Wolf J, Schwarz J, Knittler K, Murphy G, Michalek M, Garbers C, Bartsch JW, Guo S, Schacher B, Eickholz P, Chalaris A, Rose-John S, Rabe B. Shedding of Endogenous Interleukin-6 Receptor (IL-6R) Is Governed by A Disintegrin and Metalloproteinase (ADAM) Proteases while a Full-length IL-6R Isoform Localizes to Circulating Microvesicles. *J Biol Chem* 2015; 290: 26059-26071.
49. Mullberg J, Schooltink H, Stoyan T, Gunther M, Graeve L, Buse G, Mackiewicz A, Heinrich PC, Rose-John S. The soluble interleukin-6 receptor is generated by shedding. *Eur J Immunol* 1993; 23: 473-480.
50. Matthews V, Schuster B, Schutze S, Bussmeyer I, Ludwig A, Hundhausen C, Sadowski T, Saftig P, Hartmann D, Kallen KJ, Rose-John S. Cellular cholesterol depletion triggers shedding of the human interleukin-6 receptor by ADAM10 and ADAM17 (TACE). *J Biol Chem* 2003; 278: 38829-38839.
51. Luz-Crawford P, Djouad F, Toupet K, Bony C, Franquesa M, Hoogduijn MJ, Jorgensen C, Noel D. Mesenchymal Stem Cell-Derived Interleukin 1 Receptor Antagonist Promotes Macrophage Polarization and Inhibits B Cell Differentiation. *Stem Cells* 2016; 34: 483-492.
52. Gu W, Yao L, Li L, Zhang J, Place AT, Minshall RD, Liu G. ICAM-1 regulates macrophage polarization by suppressing MCP-1 expression via miR-124 upregulation. *Oncotarget* 2017; 8: 111882-111901.
53. Sahni M, Yeboah B, Das P, Shah D, Ponnalagu D, Singh H, Nelin LD, Bhandari V. Novel biomarkers of bronchopulmonary dysplasia and bronchopulmonary dysplasia-associated pulmonary hypertension. *J Perinatol* 2020; 40: 1634-1643.
54. Mansson J, Fellman V, Stjernqvist K, Group ES. Extremely preterm birth affects boys more and socio-economic and neonatal variables pose sex-specific risks. *Acta Paediatr* 2015; 104: 514-521.
55. Garbers C, Heink S, Korn T, Rose-John S. Interleukin-6: designing specific therapeutics for a complex cytokine. *Nat Rev Drug Discov* 2018; 17: 395-412.

Figure legends

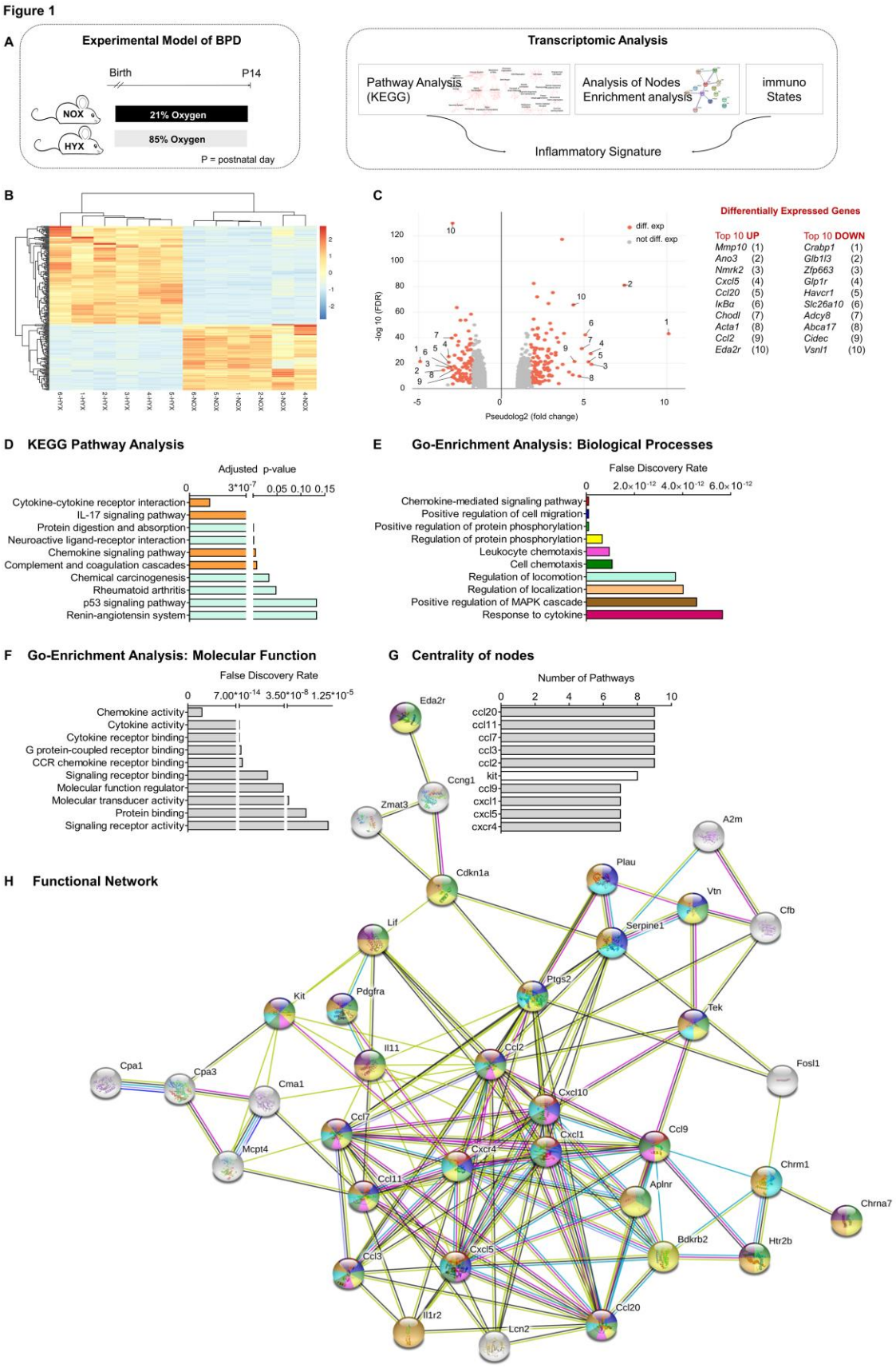

Figure 1: *Transcriptomic analyses of lungs of newborn mice exposed to normoxia (21 % O_2, NOX) or hyperoxia (80 % O_2, HYX) for 14 days (*A). Heatmap (B) and volcano plot (C). The heatmap contains only genes with an average log-fold change (FC) greater than 2 and FDR-corrected p-value < 0.01.

Genes with average log-fold change (FC) greater than 2 and FDR-corrected p-value < 0.01 were considered as differentially expressed genes (DEG) and they are colored red. Labels in the volcano plot indicate top 10 up- and down-regulated genes based on FC; n = 6 per group; NOX, normoxia (21 % O_2); HYX, hyperoxia (80 % O_2). D: KEGG pathway analysis showing the top ten pathways dysregulated in lungs of newborn mice exposed to NOX or HYX for 14 days. E-H: Functional enrichment analysis to identify functional gene sets, including biological processes (E) and molecular functions (F) using differentially expressed genes identified in the top 10 pathways of the KEGG pathway analysis. Ranking of the DEGs (G) identified as nodes by their interaction in the functional network (H); n = 6 per group.

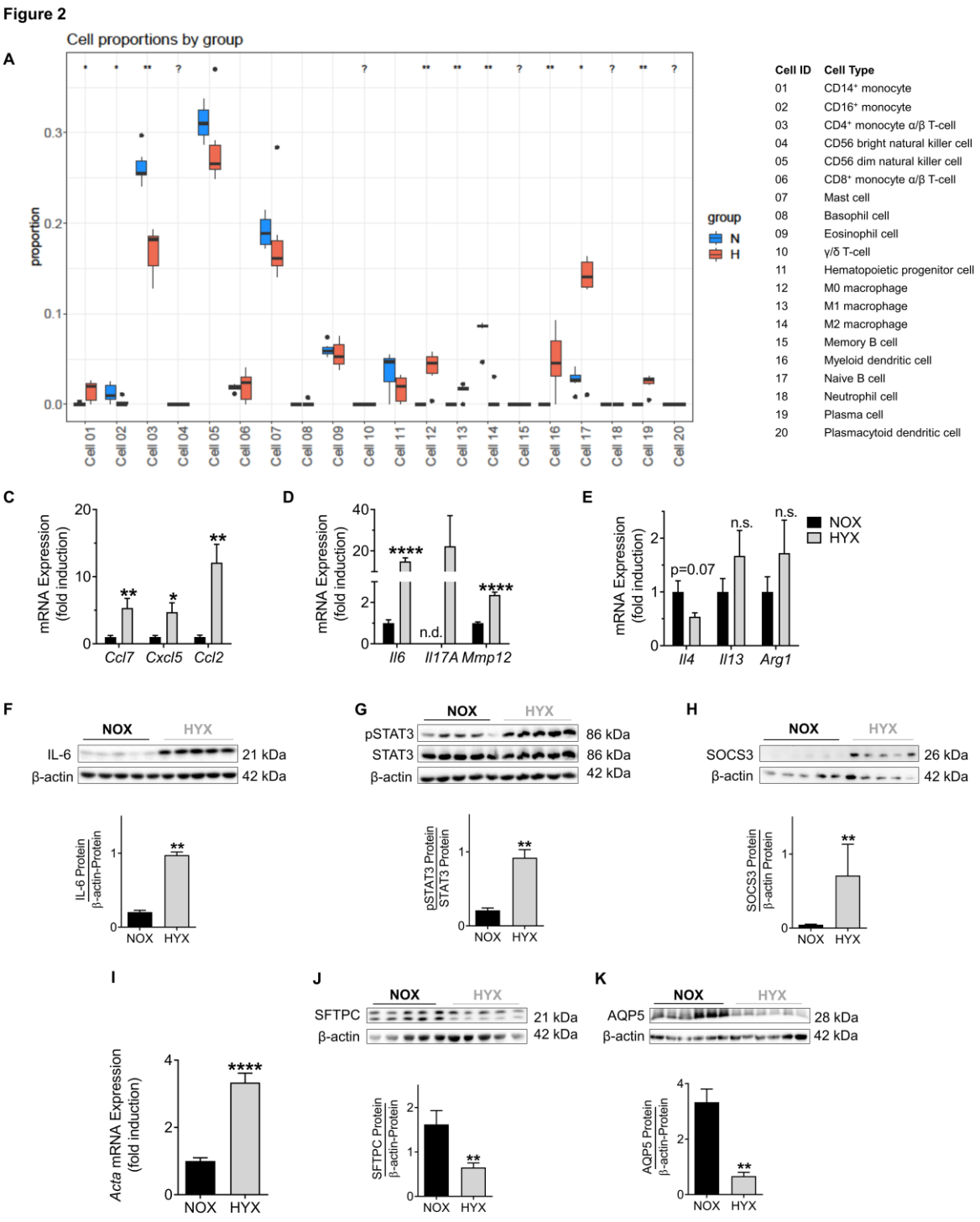

Figure 2: *Prolonged hyperoxia activates macrophages and IL-6/STAT3 signaling in neonatal lungs*. A: Immune cell type proportions in lungs of newborn mice exposed to normoxia (21 % O_2, N) or hyperoxia (80 % O_2, H) for 14 days. Cell proportions were estimated by using the immunoStates *in silico* cell deconvolution (n = 6 per group) B: List of identification numbers for each immune cell type. C-E: Newborn mice were exposed to normoxia (NOX; 21 % O_2; black bars) or hyperoxia (HYX; 85 % O_2; grey bars) for 28 days, followed by assessment of gene expression of chemokines identified

as central nodes in the functional transcriptomic network and regulating macrophage function using qRT-PCR [C; CC-chemokine ligand 7 (*Ccl7*), C-X-C motif chemokine 5 (*Cxcl5*), and *Ccl2*]. Measurement of mRNA expression of genes characteristic for M1-like polarization [D; Interleukin 6 (*Il6*), *Il17A*, and metalloproteinase 12 (*Mmp12*)] and M2-like polarization [E; *Il4*, *Il13*, and arginase 1 (*Arg1*)] using qRT-PCR (n = 6-7/group). F: Measurement of IL-6 protein abundance by immunoblot in lungs of newborn mice exposed to normoxia (NOX, 21 % O_2, black bars) or hyperoxia (HYX, 85 % O_2, grey bars) from postnatal day 1 (P1) to P28 (n = 5/group); β-actin served as loading control; the densitometric analysis is shown below the immunoblot. G, H: Phosphorylated and total STAT3 (pSTAT3, STAT3; G) as well as SOCS3 protein (H) were assessed by immunoblot; densitometric summary data show pSTAT3 relative to total STAT3 and SOCS3 relative to β-actin, which served as loading control (n = 5/group). I: Measurement of α smooth muscle actin (αsma, known as *Acta2*) mRNA as a mesenchymal marker in lungs at P28 by qRT-PCR (n = 10-12/group); gene expression is shown as fold induction. J, K: Immunoblots show epithelial cell markers at P28: surfactant protein C (SFTPC) as an indicator of alveolar epithelial type II cells (ATII) (J), and aquaporin 5 protein (AQP5) as a marker of ATI (K); β-actin served as loading control; the densitometric analysis is shown below the respective immunblot. L: Assessment of respiratory lung compliance in mice at P28 (n = 5/group). Mean±SEM; Mann-Whitney test; *p<0.05; **p<0.01; ****p<0.0001.

Figure 3

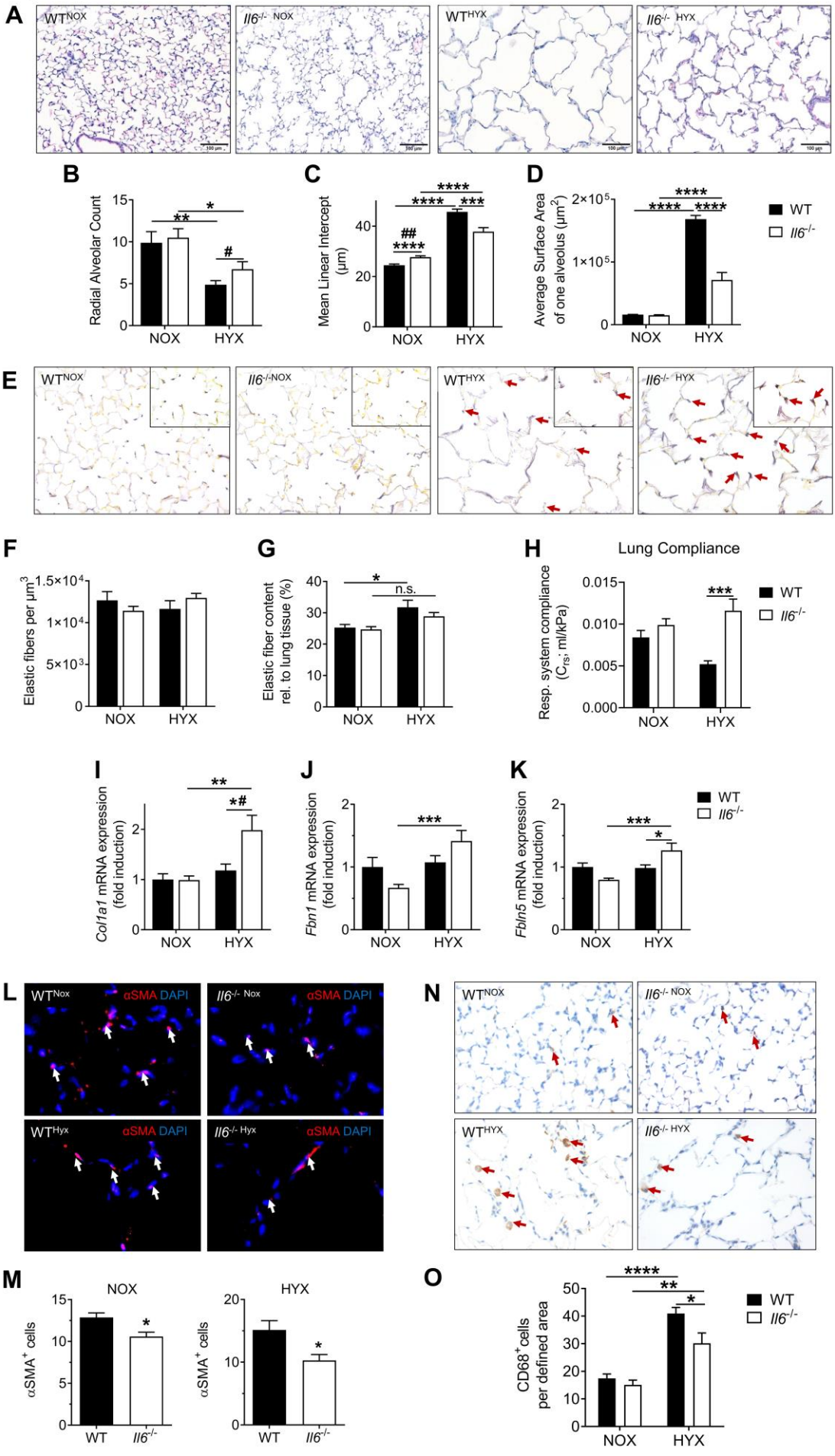
A
WTNOX
Il6-/- NOX
WTHYX
Il6-/- HYX
B
Radial Alveolar Count
NOX
HYX
C
Mean Linear Intercept (µm)
D
Average Surface Area of one alveolus (µm2)
WT
Il6-/-
E
F
Elastic fibers per µm3
G
Elastic fiber content rel. to lung tissue (%)
n.s.
H
Lung Compliance
Resp. system compliance (Crs; ml/kPa)
I
Col1a1 mRNA expression (fold induction)
J
Fbn1 mRNA expression (fold induction)
K
Fbln5 mRNA expression (fold induction)
L
WTNox
αSMA DAPI
Il6-/- Nox
WTHyx
Il6-/- Hyx
N
M
αSMA+ cells
O
CD68+cells per defined area

Figure 3: *Loss of Il6 preserves alveolar as well as elastic fiber formation, and reduces macrophage invasion in neonatal lungs after hyperoxia*. A: Representative images of hematoxylin and eosin (H&E) stained tissue sections showing alveolarization in mice at postnatal day 28 (P28). Wildtype (WT) and Interleukin 6 (*Il6*) knockout mice ($Il6^{-/-}$) were exposed to hyperoxia (HYX, 85 % O_2) or normoxia (NOX, 21 % O_2) from postnatal day 1 (P1) to P28. B-D: Summary data of quantitative histomorphometric analyses: radial alveolar count (RAC; B), mean linear intercept (MLI, C), surface of a single alveolus (alveolar surface area; D). E: Representative images of Hart's-stained tissue sections showing distribution and localization of elastic fibers in mice at P28. Arrows indicate elastic fibers at the secondary tips after hyperoxia. F, G: Summary data of quantitative analyses of elastic fibers per defined area (μm^3) (F) and elastic fiber content relative to lung tissue in % (G). H: Measurement of respiratory system compliance using whole body plethysmography in $Il6^{-/-}$ and WT mice at P28. I-K: Assessment of the expression of genes encoding components of lung matrix, including elastic fibers: Collagen 1α1 (*Col1a1*), Fibrillin 1 (*Fbn1*), and Fibulin5 (*Fbln5*). L, M: Representative immunofluorescent stainings of αSMA as a marker of myofibroblasts. White arrows depict positive stained cells (L); Quantification data of αSMA^+ cells relative to all $DAPI^+$ cells (M). N, O: Representative images of macrophage using CD68 staining. Red arrows depict positive stained cells (N). Quantification data of $CD68^+$ cells per field of view (O). Mean±SEM; n = 4-9/group; Mann-Whitney test: $^{\#}p<0.05$; $^{\#\#}p<0.01$. Two-way ANOVA: *p<0.05; **p<0.01; ***p<0.001; ****p<0.0001; n.s. = not significant.

Figure 4

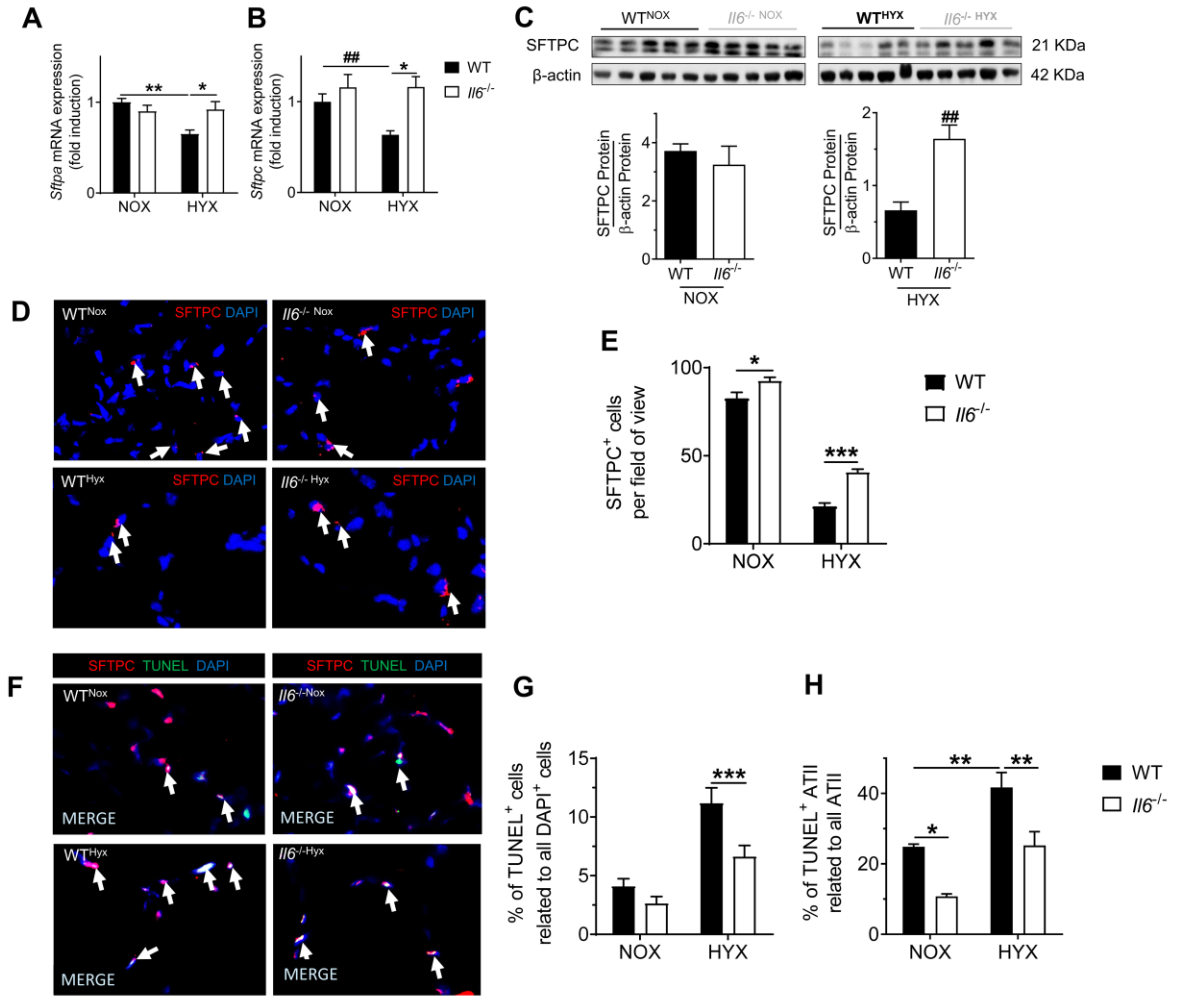

Figure 4: *Loss of Il6 protects alveolar epithelial type II cells (ATII) in lungs of newborn mice after exposure to prolonged hyperoxia*. Wildtype (WT) and Interleukin 6 knockout mice (*Il6*$^{-/-}$) were exposed to hyperoxia (HYX, 85 % O_2) or normoxia (NOX, 21 % O_2) from postnatal day 1 (P1) to P28. A, B: Assessment of expression of genes encoding surfactant proteins (*Sftp*) in lungs at P28: *Sftpa* (A) and *Sftpc* (B). C: Immunoblot showing surfactant protein C (SFTPC) protein abundance in lungs at P28; SFTPC protein was related to β-Actin, which served as loading control; densitometric data are displayed below the respective immunoblot. D: Representative immunofluorescence stainings for surfactant protein C (SFTPC, red) as an indicator of ATII in lungs at P28; DAPI was used for nuclear staining. SFTPC$^+$ cells are indicated with white arrows. E: Quantitative data summary of SFTPC$^+$ cells per field of view. F-H: Representative Co-immunofluorescence staining for TUNEL as an indicator of cell death (green) and SFTPC (red) in lungs at P28; DAPI was used for nuclear staining (F). Quantitative summary data of the percentage of

TUNEL^{+} cells (G), and TUNEL^{+} ATII relative to all ATII (H). Mean±SEM; n = 4-9/group. Mann-Whitney test: $^{\#\#}p<0.01$ or as indicated; Two-way ANOVA followed by Dunn's post test: *p<0.05; **p<0.01; ***p<0.001.

Figure 5

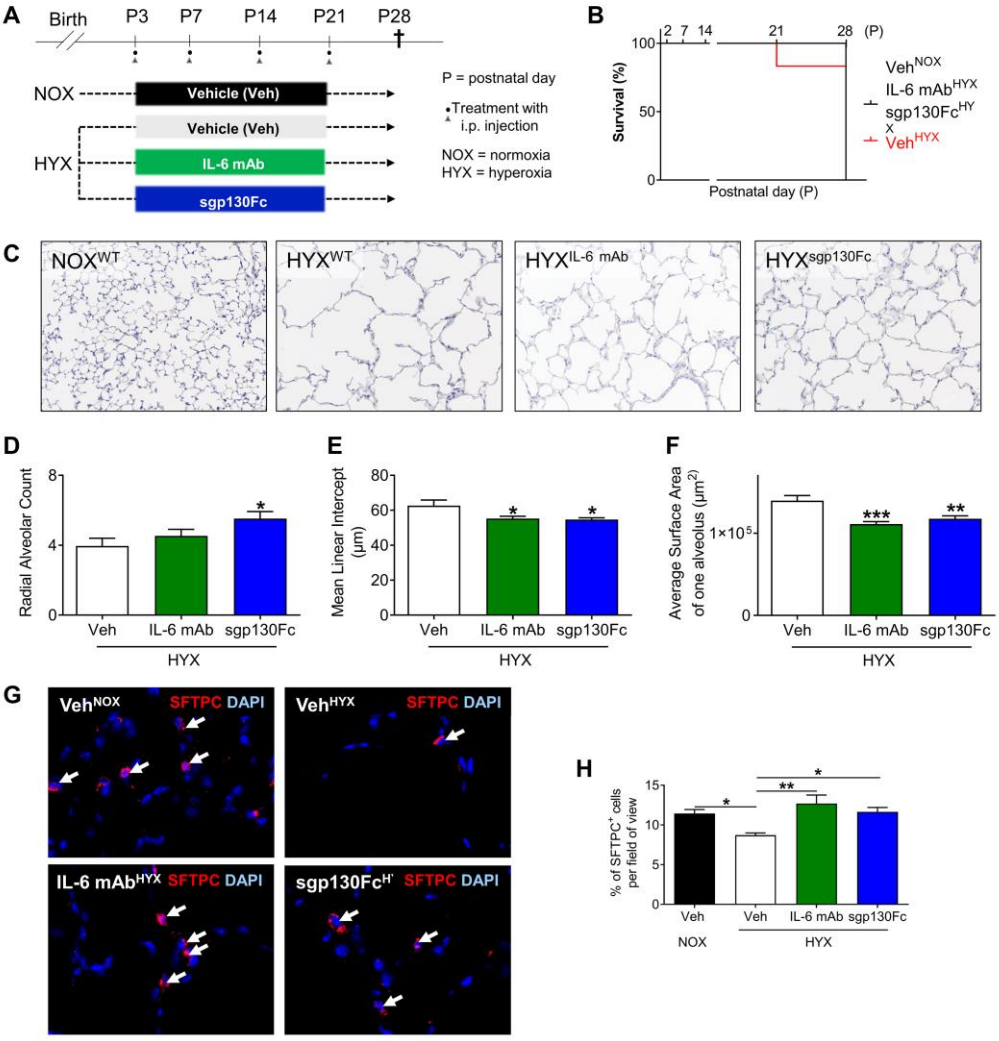

Figure 5: *Inhibition of global Interleukin 6 (IL-6) signaling and IL-6 trans-signaling enables lung growth and promotes ATII survival in lungs of newborn mice exposed to prolonged hyperoxia*. A: Scheme of the experimental design. Wildtype (WT) mice were exposed to hyperoxia (HYX, 85 % O_2) from postnatal day 1 (P1) to P28; mice were treated i.p. with vehicle, IL-6 mAb or sgp130Fc. B: Survival curve from birth until P28: vehicle-treated mice in NOX; vehicle-treated mice in HYX; IL-6 mAb-treated mice in HYX; and sgp130Fc-treated mice in HYX. C: Representative images of hematoxylin and eosin (H&E) stained tissue sections showing alveolarization in mice at P28. D-F: Summary data of the quantitative histomorphometric analysis: radial alveolar count (RAC, D), mean linear intercept (MLI, E), and surface of a single alveolus (alveolar surface area; F). G: Representative immunofluorescence stainings for surfactant protein C (SFTPC, red) as an indicator of alveolar epithelial cells type II (ATII) in lungs at P28; DAPI was used for nuclear staining. $SFTPC^+$ cells are indicated with white arrows. H: Quantitative data summary of $SFTPC^+$ cells per field of

view. Mean±SEM; n = 4-6/group; One-way Anova followed by Bonferroni's post-test: *$p<0.05$; **$p<0.01$; ***$p<0.001$.

Figure 6

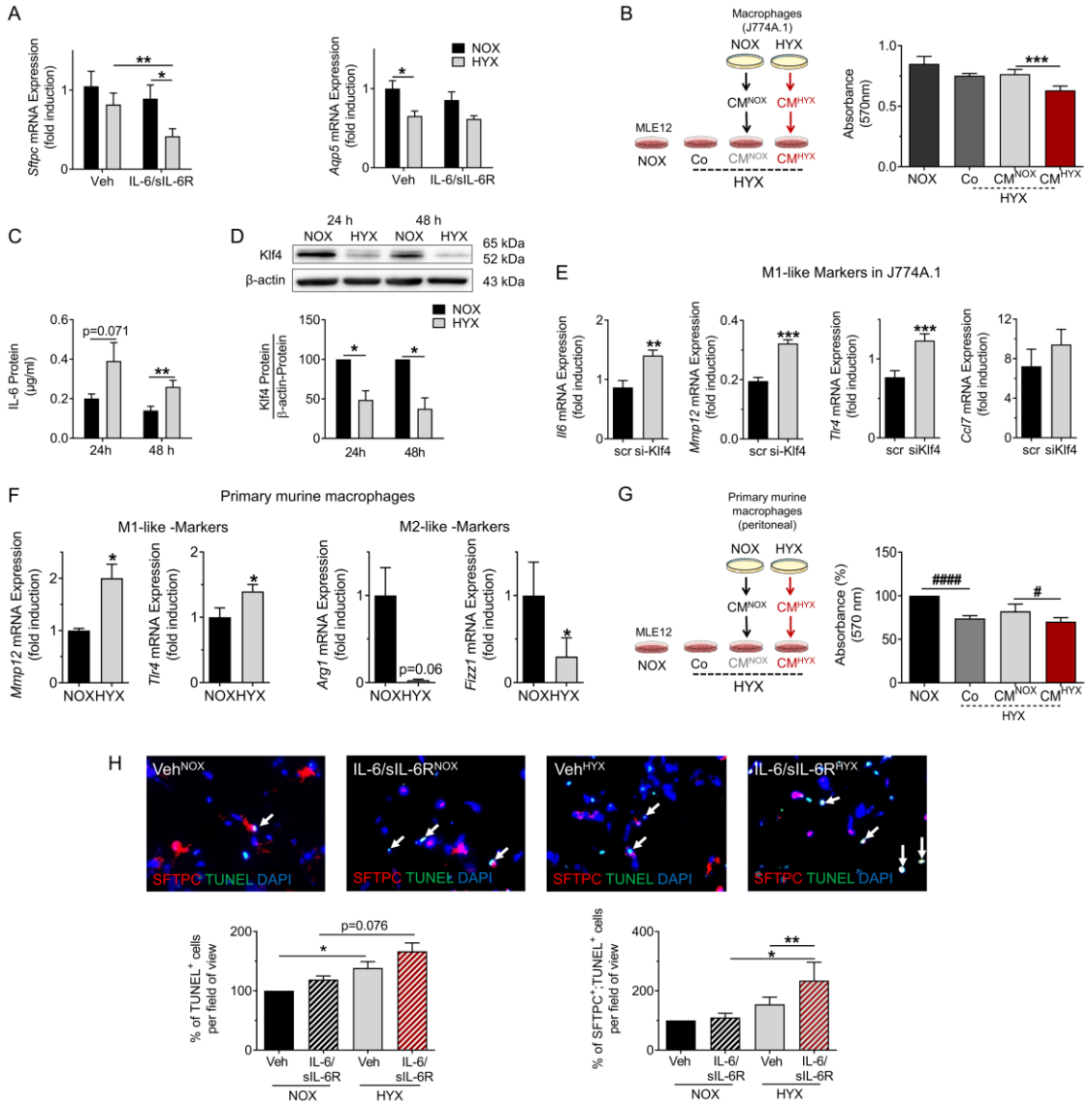

Figure 6: *Hyperoxia-conditioned murine macrophages and IL-6/sIL-6R trigger hyperoxia-induced apoptosis of ATII.* A: Assessment of gene expression of surfactant protein C (*Sftpc*) and aquaporin 5 (*Aqp5*) in murine lung epithelial cells (MLE12). MLE12 were cultured in serum-rich medium, followed by serum-reduced medium for 12 h. Afterwards the cells were treated either with vehicle (Veh) or IL-6/soluble IL-6 receptor (IL-6/sIL-6R) and exposed to hyperoxia (HYX, 85 % O_2) or normoxia (NOX, 21 % O_2) for 24 h; n = 11/group; β-actin served as housekeeping gene. B: Scheme depicting the experimental design: macrophages (J774.A1) were exposed to NOX or HYX for 48 h; subsequently MLE12 were exposed to HYX and treated with conditioned medium (CM) of NOX-exposed macrophages (CM^{NOX}), CM^{HYX} or vehicle (untreated medium, Co) for 24 h; Control MLE12 were exposed to NOX. At the end, proliferation of MLE12 was assessed using MTT assay; n = 12-

30/group. C: Measurement of Interleukin 6 (IL-6) protein using ELISA in supernatants of J744.A1 macrophages. J744.A1 were cultured in serum-rich medium, followed by exposure to HYX or NOX for 24 h and 48 h; n = 8/group. medium D: Immunoblot showing Klf4 protein abundance in macrophages (J774.A1) after exposure to NOX or HYX for 24 h or 48 h; Klf4 protein was related to β-Actin, which served as a loading control; densitometric data are displayed under the immunoblot; n = 4-5/group. E: Klf4 was suppressed in macrophages (J744.A1). Cells were transfected with siRNA against Klf4 (si-klf4) or scrambled siRNA (scr) using endo-porter technique, followed by a recovery time of 24 h in serum-rich medium. Subsequently, cells were starved with serum-reduced medium. Gene expression of macrophage markers was assessed after exposure to HYX for 48 h: *Il6*, metalloproteinase 12 (*Mmp12*), Toll like receptor 4 (*Tlr4*), and CC-chemokine ligand 7 (*Ccl7*); β-actin served as housekeeping gene; Mean±SEM; n = 4-5/group. F: Primary murine macrophages (peritoneal) were isolated and cultured for 24 h in serum-rich medium. Subsequently, cells were exposed to NOX or HYX for 48 h in serum-reduced medium. Gene expression of M1-like (*Mmp12*, *Tlr4*) and M2-like [*Arg1*, Resistin-like molecule alpha1 (*Fizz1*)] markers were assessed using qRT-PCR; β-actin served as housekeeping gene. G: Similar to (B) primary murine macrophages were exposed to NOX or HYX for 48 h; subsequently MLE12 were exposed to HYX and treated with CM^{NOX}, CM^{HYX} or vehicle (untreated medium, Co) of primary murine macrophages; control MLE12 were exposed to NOX. After 24 h, proliferation of MLE12 was assessed using MTT assay; n = 12-30/gr. H: Precision-Cut Lung Slices (PCLS) of 14-days old mice were treated either with vehicle (Veh) or IL-6/soluble IL-6 receptor (IL-6/sIL-6R) and exposed to NOX or HYX for 48 h; n = 3-4 /group. Representative co-immunofluorescence staining for TUNEL as an indicator of apoptosis (green) and SFTPC (ATII, red) along with quantitative summary data of the percentage of $TUNEL^+$ and $SFTPC^+$;$TUNEL^+$ cells relative to all ATII; Mean±SEM; paired t-test: *p<0.05, **p<0.01, ***p<0.001; repeated measures (RM) One-way ANOVA followed by Bonferroni's post-test: $^{\#}$p<0.05, $^{\#\#\#\#}$p<0.0001.

Figure 7

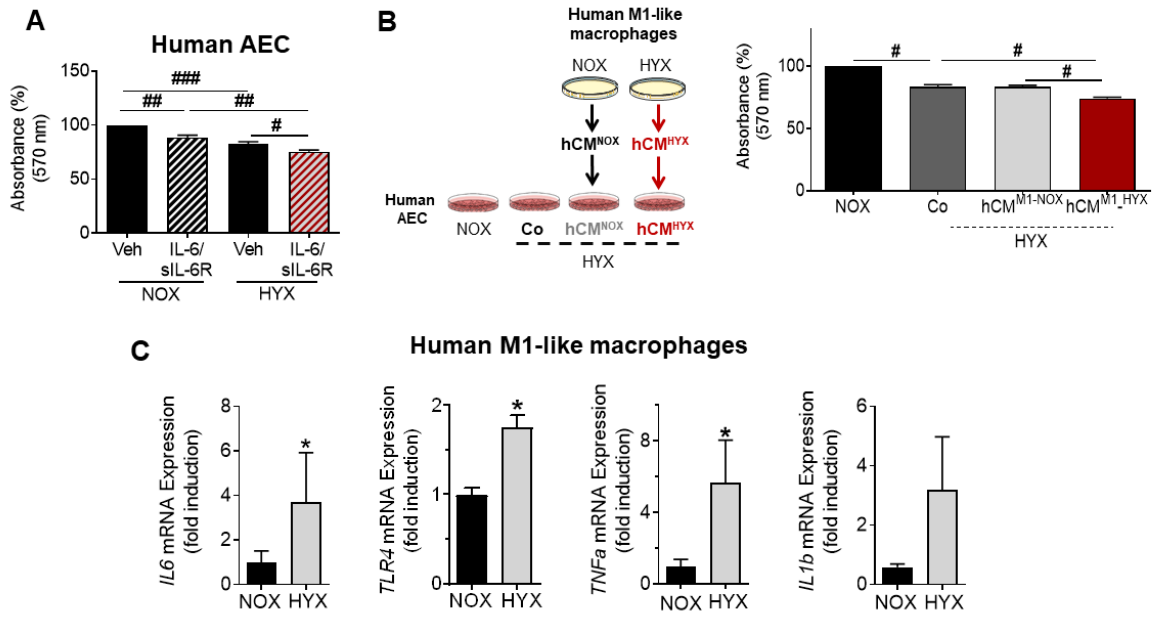

Figure 7: *IL-6/sIL-6R and human M1-like macrophages adversely affect human alveolar epithelial cell (hAEC) homeostasis*. A: Assessment of proliferation of human alveolar epithelial cells (hAEC) was assessed using MTT assay; hAEC were cultured in serum-rich medium for 24 h. Afterwards the cells were treated either with vehicle (Veh) or IL-6/soluble IL-6 receptor (IL-6/sIL-6R) and exposed to hyperoxia (HYX, 85 % O_2) or normoxia (NOX, 21 % O_2) for 24 h; n = 6/group. B: Scheme depicting the experimental design: human M1-like macrophages were exposed to NOX or HYX for 48 h and conditioned medium (CM) was collected; subsequently, hAECs were treated under HYX with CM of human NOX-exposed macrophages (hCM^{NOX}), hCM^{HYX} or vehicle (Co) for 24 h; control hAECs were exposed to NOX. At the end, proliferation of hAEC was assessed using MTT assay; n = 4 /group. C: Human monocytes were isolated from blood and treated with Granulocyte macrophage-colony stimulating factor (GM-CSF, 100ng/ml) in serum-rich medium for seven days. Subsequently, cells were maintained in serum-reduced medium and exposed to NOX or HYX for 48 h, followed by assessment of expression of genes encoding for macrophage markers [Interleukin 6 (h*IL6*), Toll like receptor 4 (*TLR4*), Tumor necrosis factor alpha (*TNFa*), and Interleukin1b (*IL1b*)] using qRT-PCR; β-actin served as housekeeping gene. Mean±SEM; n = 4-5/group; Repeated measures (RM) One-way ANOVA with Bonferroni's post-test: $^{\#}p<0.05$; $^{\#\#}p<0.01$; $^{\#\#\#}p<0.001$; Wilcoxon paired t-test: *p<0.05.

Figure 8

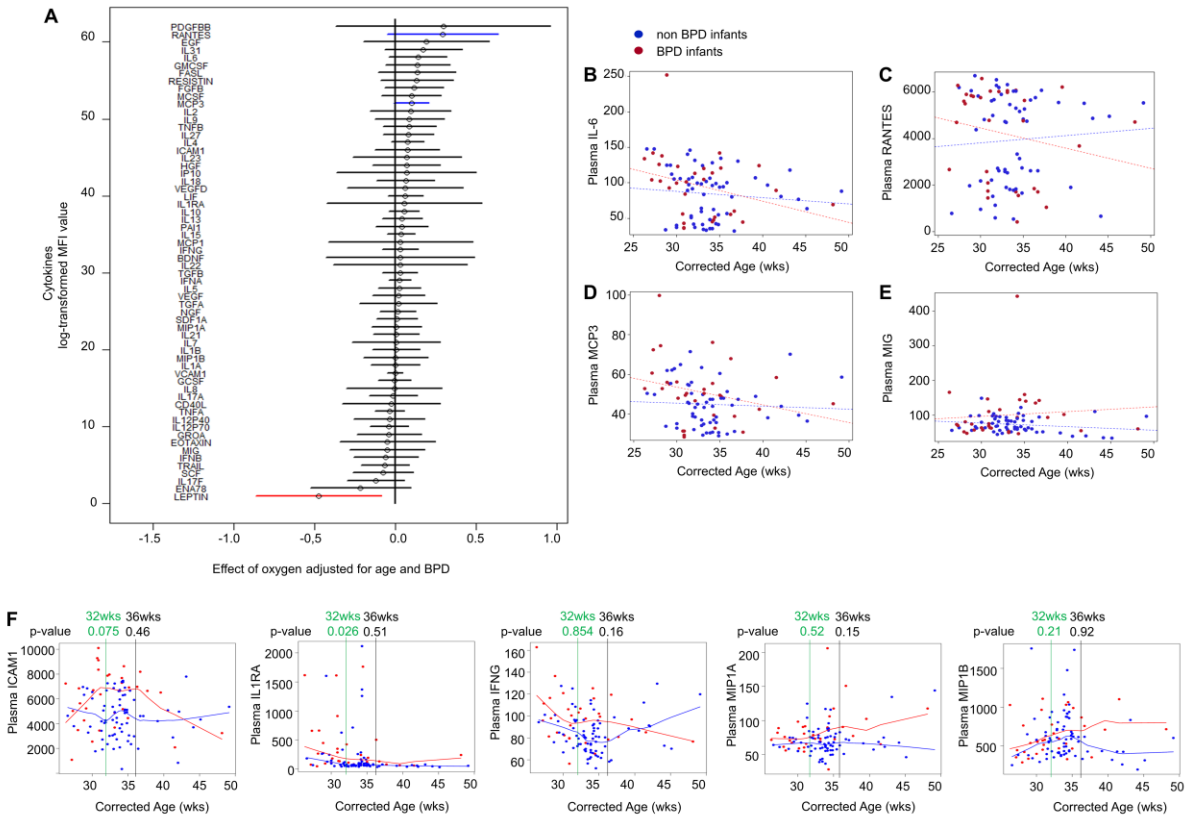

Figure 8: *Clinical data showing the dynamic of cytokine concentrations in plasma of infants with and without BPD.* A: Forest plot displaying the effect of oxygen on cytokine concentrations in premature infants (n = 55). Data were adjusted for age and BPD. Plasma cytokines were measured using multiplex assay; blue and red lines highlight most upregulated and downregulated cytokines. B-E: Mixed linear modelling to show a longitudinal pattern of changes in plasma cytokine levels in infants that progressed to BPD (red dots) versus non-BPD (blue dots). Plasma Interleukin 6 (IL-6) (B); and macrophage related cytokines (C-E): RANTES (C; CC-chemokine ligand 5, CCL5), MCP3 (D; monocyte-chemotactic protein 3; CC-chemokine ligand 7, CCL7); and MIG [E; Monokine-induced by gamma interferon; chemokine (C-X-C motif) ligand 9]. F: nonparametric fitted curve for intercellular adhesion molecule 1 (ICAM; CD54), Interleukin 1 receptor antagonist (IL1RA), Interferon gamma (IFNG), macrophage inflammatory protein α (MIP1A; CCL3; p=0.15), and MIP1B (CCL4). Statistical differences between BPD and non-BPD infants were tested at 32 weeks (green line) and 36 weeks (black line). The respective p-values are indicated.

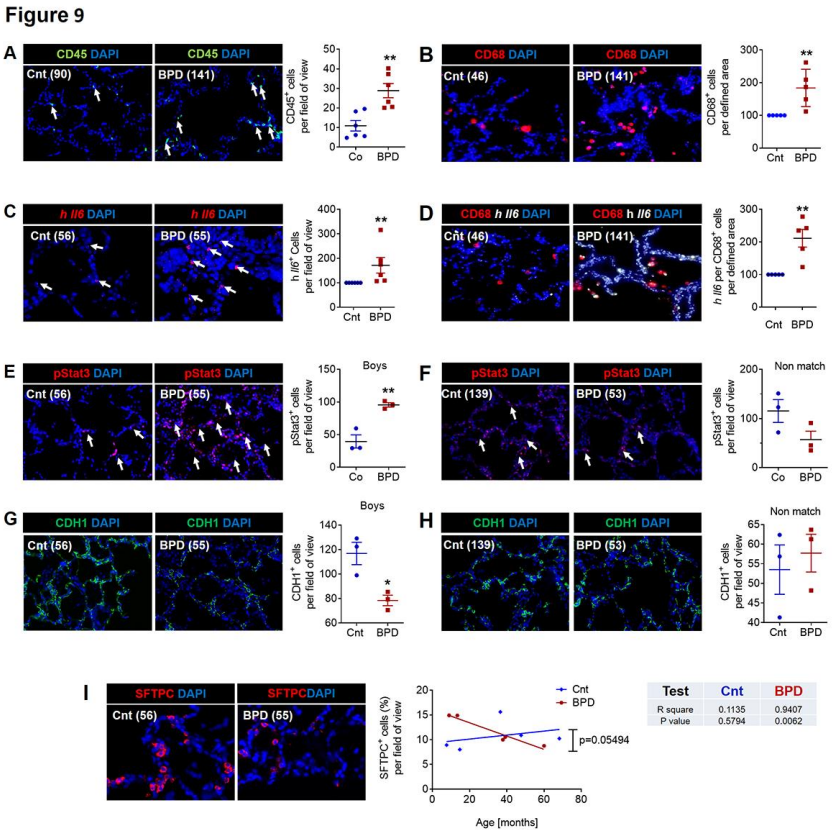

Figure 9: *Inflammation and Interleukin 6 (IL-6)/STAT3 signaling in lungs of infants with BPD and non-BPD (Control, Co).* A: Representative immunofluorescent staining for immune cells using CD45 as a marker (green) in age-matched BPD and control lungs (Co); the lung identification number of the infants are indicated in brackets. Immune cells ($CD45^+$ cells) were counted in 4-12 fields of view per lung. Summary data of the quantification of immune cells ($CD45^+$ cells) per field of view for all infants (n = 6/group). B: Representative co-immunofluorescent localization of CD68 (marker of macrophages, red) in age-matched BPD and Co lungs; white arrows are indicating $CD68^+$ cells. The analysis of $CD68^+$ cells per 6-12 fields of view is shown next to the images; n = 6 group. C: Representative localization of human *IL6* (*hIL6*, red) in lungs with BPD and Co; white arrows are indicating h$IL6^+$ *in situ* hybridization. The analysis of h$IL6^+$ cells per 6-12 fields of view is shown next to the images; n = 6 group. D: Representative co-immunofluorescent localization of CD68 (marker of macrophages, red) with *hIL6* (white; *in situ* hybridization) in age-matched BPD and Co lungs; white arrows are indicating $CD68^+$ and h$Il6^+$. The analysis of h*IL6* mRNA expression per $CD68^+$ cells per 6-12 fields of view is shown next to the images; n = 6 group. E, F: Representative immunofluorescent staining showing pSTAT3 positive staining in lungs with BPD and Co; white arrows indicate $pSTAT3^+$ cells. The analysis of $pSTAT3^+$ cells in 4-12 field of view was performed

for sex- and age matched BPD and control lungs (E; boys; n = 3/group) as well as for age-matched, but not sex-matched BPD and control lungs (F; n = 3/group). The graph is shown next to the respective images. G, H: Representative immunofluorescent staining showing CDH1 (green) positive staining in BPD and control lungs. The analysis of $CDH1^+$ cells in 4-12 fields of view was performed for sex- and age matched BPD and control lungs (G; boys; n = 3/group) as well as for age-matched, but not sex-matched BPD and control lungs (H; n = 3/group). The graph is shown next to the respective images. I: Representative immunofluorescent of SFTPC [marker of alveolar epithelial type II cells (ATII), red] in BPD and Co lungs; The analysis of linear regression for the amount of $SFTPC^+$ and age is shown in the graph (BPD, red; Co, blue); r^2 and p-value are indicated next to the graph; n = 5/group. Mean±SEM; Mann-Whitney test or Student's t-test: *$p<0.05$; **$p<0.01$.

Figure 10

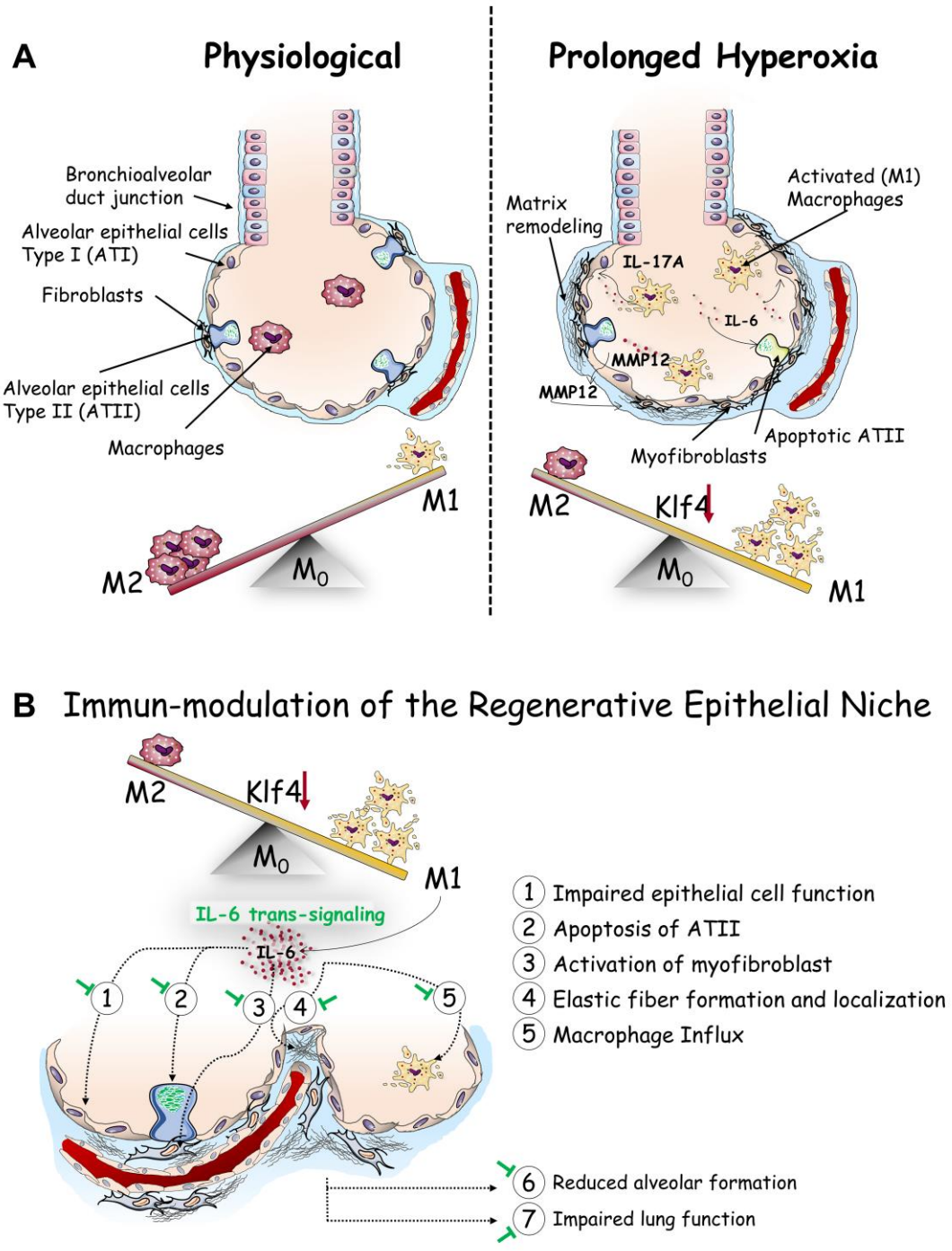

Figure 10: *Proposed working model* illustrating how hyperoxia induces macrophage polarization. A: The M1-like-driven inflammatory phenotype leads to the secretion of cytokines, such as IL-6 and IL17A, as well macrophage elastase, also known was metalloproteinase 12 (MMP12). This inflammatory alveolar microenvironment reduces survival of alveolar epithelial type II cells (ATII), whereas fibroblasts are activated and matrix remodelling promoted. B: Polarization of macrophages following hyperoxia leads to a release of IL-6, which adversely affects the regenerative epithelial

niche. However, IL-6 deficiency protects from these changes by (1) promoting expression of surfactant proteins and (2) survival of ATII; (3) reducing myofibroblasts; (4) protecting from perturbed elastic fiber assembly and localization; and (5) attenuating macrophage influx. These beneficial effects of IL-6 deficiency on the alveolar compartment enables (6) alveolar formation, and (7) protects from reduced lung function, offering a new therapeutic target to treat BPD.

Table 1 Healthy Human Sample

Donor Id	Calculated Age (Months)	Sex	Race	ClinPathDx: Control
D075	4.00	Male	White	Normal growth and development
D031	7.64	Male	White	Normal growth and structure
D090	14.70	Female	NR	Normal growth and structure
D046	36.5	Male	White	Normal growth and development
D139	47.67	Female	1 race	Normal lung growth and structure
D056	68.21	Male	White	Normal growth and development

BPD Human Sample

Donor Id	Calculated Age (Months)	Sex	Race	ClinPathDx: BPD/CLD
D029	3.55	Male	White	23 wk at birth, Histo: CLD/BPD with lobular remodeling; Mild mediuml hypertrophy of small arteries
D086	8.94	Male	White	25 wk at birth, probable BPD w/ resp failure
D141	13.40	Male	White	25 wk at birth, BPD; mod deficient alveolarization, chronic inflammation, airway muscle hyperplasia, mediuml hypertrophy of small arteries
D039	39.13	Female	NR	23 wk at birth, "new" BPD
D053	37.87	Male	White	24 wk at birth, BPD, mild-mod bronchiolitis
D055	59.96	Male	White	32 wk at birth, possible mild BPD, asthma, mod bronchopneumonia

Table 1: Clinical data of lungs of infants with and without bronchopulmonary dysplasia (BPD).

Macrophage-derived IL-6 trans-signaling as a novel target in the pathogenesis of bronchopulmonary dysplasia

Dharmesh Hirani[1,2], Cristina M. Alvira[3], Soula Danopoulos[4], Carlos Milla[3], Michele Donato[5], Lu Tian[6], Jasmine Mohr[1,2], Katharina Dinger[1,2], Christina Vohlen[1,7], Jaco Selle[1], Silke v. Koningsbruggen-Rietschel[7], Verena Barbarino[8], Christian Pallasch[8], Stefan Rose-John[9], Margarete Odenthal[10], Gloria S. Pryhuber[11], Siavash Mansouri[12], Rajkumar Savai[12,13], Werner Seeger[12, 13], Purvesh Khatri[5], Denise Al Alam[4], Jörg Dötsch[7], Miguel A. Alejandre Alcazar[1,2,13,14]

[1]University of Cologne, Faculty of Medicine and University Hospital Cologne, Translational Experimental Pediatrics - Experimental Pulmonology, Department of Pediatric and Adolescent Medicine, Germany; [2]University of Cologne, Faculty of Medicine and University Hospital Cologne, Center for Molecular Medicine Cologne (CMMC), Germany; [3]Department of Pediatrics, Stanford University School of Medicine, Stanford, CA, USA; [4]Lundquist Institute for Biomedical Innovation at Harbor-UCLA Medical Center , Torrance, CA, United States; [5]Biomedical Informatics Research-Institute for Immunity, Transplantation, and Infection, Stanford University, Stanford, California; [6]Department of Biomedical Data Science, Stanford University, Stanford, USA; [7]University of Cologne, Faculty of Medicine and University Hospital Cologne, Department of Pediatric and Adolescent Medicine, Germany; [8]Department I of Internal Medicine, Center for Integrated Oncology (CIO) Köln-Bonn, University of Cologne, Germany, [9]Institute of Biochemistry, Christian-Albrechts-University Kiel, Germany; [10]University of Cologne, Faculty of Medicine and University Hospital Cologne, Institute for Pathology, Germany; [11]Division of Neonatology, Department of Pediatrics, University of Rochester Medical Center, Rochester, NY, USA. [12]Department of Lung Development and Remodeling, Max-Planck-Institute for Heart and Lung Research, Member of the German Center for Lung Research (DZL), Bad Nauheim, Germany; [13]Institute for Lung Health (ILH), University of Giessen and Marburg Lung Center (UGMLC), Member of the German Center for Lung Research (DZL), [14]University of Cologne, Faculty of Medicine and University Hospital Cologne, Cologne Excellence Cluster on Stress Responses in Aging-associated Diseases (CECAD), Cologne, Germany.

Summary: M1-like macrophage activation is linked to IL-6/STAT3 axis in clinical and experimental BPD. Inhibition of macrophage-related IL-6 trans-signaling promotes ATII survival and lung growth in experimental BPD as a new therapy for preterm infants.

Online Data Supplement

Material and Methods

Animal studies

All animal studies were approved by the local government authorities (LANUV, NRW, Germany; 87-51.04.2010.A372; 84-02.04.2015.A120; 84-02.04.2016.A119). Adult and neonatal male and female C57BL/6N and C57BL/6J (WT) and B6.129S2*Il6*tm1Kopf/J (*Il6*$^{-/-}$) mice were housed in humidity- and temperature-controlled rooms exposed to a 12 h dark/light cycle and were allowed food and water ad libitum.

Neonatal hyperoxia-induced lung injury model

Newborn mice were pooled and randomized to dams at the day of birth (born within 12 h of each other). Half of the litters were exposed to 85 % or 40 % O_2 (hyperoxia, HYX) for 3, 7, and 28 days, whereas the other pups were at room air [21% O_2; normoxia, NOX] as described previously (1). Every 24 h the nursing dams were rotated between hyperoxia and normoxia litters to avoid O_2-related toxic effects on the dams. Exposure to hyperoxia was performed in a 90 × 42 × 38 cm plexiglas chamber. Oxygen concentrations were monitored with a Miniox II monitor (Catalyst Research, Owing Mills, MD).

Treatment with sgp130Fc and IL-6 mAb

To determine if inhibition of IL-6 signaling protects from neonatal hyperoxia-induced lung injury and promotes alveolarization, newborn wildtype (C57Bl/6N) mice were treated with intraperitoneal injection of either sgp130Fc (~10µg/g bw), IL-6 mAb (~10µg/g bw) or vehicle (PBS) at postnatal day 3 (P3), P7, P14, and P21. At P28, mice were sacrificed. The dose was based on previous studies (2).

Mouse model of hyperoxic lung injury for RNA Seq

All animal procedures were approved by the Institutional Animal Care and Use Committee (IUCAC) at Stanford University. As part of a separate study, mice contain loxP sites flanking critical exons of the Ikk2 (IKKβ) gene, described previously (3), were crossed to transgenic $Pdgfb^{WT}$ and $Pdgfb^{CreERT2}$ mice (4), which express a tamoxifen inducible form of Cre-recombinase under the control of the *Pdgfb* promoter, to generate $Ikk\beta^{WT}$ and $Ikk^{\Delta Endo}$ mice. For these studies, within 24 h of birth, male and female $Ikk\beta^{WT}$ pups were exposed to 80 % O_2 (hyperoxia) or 21 % O_2 (normoxia) for two weeks (P14), after receiving 300 µg of 4-OHT suspended in corn oil via daily intragastric injection from P1-P3.

RNA-Seq

Lungs were obtained from $Ikk\beta^{WT}$ pups maintained in normoxia or hyperoxia for 14 days. The pulmonary circulation was perfused with saline, and total RNA extracted using RNeasy Mini kit (Qiagen, Germantown, MD). RNA-sequencing was performed by Quick Biology (Pasadena, CA). Briefly, RNA integrity was confirmed by Agilent Bioanalyzer 2100, and libraries were prepared according to KAPA Stranded mRNA-Seq poly(A) selected kit (KAPA Biosystems, Wilmington, MA). Final library quality and quantity was analyzed, and 150 bp paired end reads sequenced on Illumina HighSeq 4000 (Illumina Inc., San Diego, CA). Reads were mapped to the latest UCSC transcript set using Bowtie2 version 2.1.0 (5), and the gene expression was estimated using RSEM v1.2.15 (6). TMM (trimmed mean of M-values) was used to normalize the gene expression. Differentially expressed genes were identified using edgeR (7). Genes showing altered expression with $p< 0.05$ and more than 1.5-fold change were considered differentially expressed.

Pulmonary function test

To assess airway resistance at P28, we used direct plethysmography for mice (FinePointe™RC; Buxco, Wellington, NC, USA) as previously described (8-10). First, mice were deeply anesthetized by intraperitoneal injection of ketamine (100 mg/kg body weight) and xylazine (5 mg/kg body weight), followed by tracheotomy and ventilation. Respiratory system compliance (Cdyn) was measured at baseline.

Tissue preparation

Mice were sacrificed as previously described (11). Lungs were excised; the right lung was immediately snap-frozen for subsequent molecular assessment; the left lung was pressure-fixed in 4 % paraformaldehyde (PFA) in phosphate-buffered saline (PBS) as described below.

Tissue assays

Protein extraction and immunoblots: After isolation of lungs, lungs were snap frozen and stored at -80 °C for protein extraction; lungs were homogenized with Chaps buffer along with 1x Halt™ protease and phosphatase inhibitor cocktail (Cat. No. 78442, Rockford, USA) using a plastic pistil. Afterwards, sonication (Bandelin, SONOPULS HD 2070, Germany) was performed for separation of tissue cells. Samples were placed on ice for 1 h, followed by centrifugation and collection of the supernatant. The protein concentration was measured using BCA Protein assay (Pierce, Thermo Fisher Scientific, #23225, Rockford, USA). For SDS-PAGE, 20-40 µg of protein was incubated with sample loading buffer at 70 °C for 10 min, and loaded on a 10 % acrylamide gel. The gel was then transferred onto a 0.45 µm nitrocellulose membrane (Amersham™ Protran® 0.45 NC nitrocellulose, GE Helathcare, #10600002, MA, USA) using semi-dry electro-blotter (Avantor, #700-1220, Vienna, Austria); blocking of the membrane was performed with 5 % milk and 2 % bovine

serum albumin (BSA) in TBS-Tween (0.1 % Tween®20, Sigma Aldrich, #P1379, Germany). The blot was then incubated with the following primary antibodies at 4 °C overnight: rat anti-interleukin 6 (IL-6; R&D System, #MAB406, Minneapolis, USA, 1:2000), rabbit anti-phosphorylated signal transducer and activator of transcription 3 (pSTAT3; Cell Signaling, #9145, Danvers, USA, 1:1000), rabbit anti-signal transducer and activator of transcription 3 (STAT3; Cell Signaling, #9139, Danvers, USA, 1:1000), rabbit anti-suppressor of cytokine signaling 3 (SOCS3; Abcam, Cat.No.ab16030, UK, 1:1000), rabbit anti-pro-surfactant protein C (SFPTC; Merck, Cat.No.AB3786, Germany, 1:2000), rabbit anti-Aquaporin 5 (AQP5; Sigma-Aldrich,Cat. No. A4979, USA, 1:2000), rabbit anti-Krüppel-like factor 4 (Klf4; Cell Signaling, #4038, Danvers, USA, 1:1000), mouse anti-β-actin (Cell Signaling, #3700, Danvers, USA, 1:10,000). Next, horseradish-peroxidase (HRP)-linked secondary antibody (anti-mouse IgG, HRP-linked antibody #7076 or anti-rabbit IgG, HRP-linked antibody #7074, Cell Signaling, Danvers, MA, USA) was applied at RT for 1 h. The membrane was then incubated with ECL™ (GE Healthcare, #RPN2232, UK) for 1 min. Protein bands were visualized by UV imager (Bio-Rad Universal Hood II Gel Doc, Cambridge, MA, USA). Densitometry analysis was performed to quantify protein amounts using Image Lab software 5.2.1 (BioRad, Germany).

RNA extraction and qRT-PCR: Lung tissue, mouse lung epithelial cells (MLE12), mouse ascites macrophages (J774A.1), primary murine macrophages (peritoneal), and human macrophages were used for RNA extraction. Samples were treated with TRI Reagent® (Sigma-Aldrich, cat. No. T9424, Germany) for cell lysis. The mRNA was precipitated by using isopropanol, washed with ethanol, and finally dissolved in RNAse free water. The mRNA concentration was measured by using Nano Quant (Tecan Infinite® 200 PRO, Switzerland), and 1 µg of mRNA was used for cDNA synthesis. To this end, mRNA was first treated with RQ1 DNase 10x Reaction Buffer (Promega, #M198A, Madison, USA) and RQ1 RNase-Free DNase (Promega, #M610A, Madison, USA) to remove genomic DNA. DNase

activity was stopped by adding DNase Stop Solution (Promega, #M199A, Madison, USA) and heating samples at 65 °C for 5 min. Random and oligo primers were added to the samples and heated at 70 °C for 15 min. Finally, M-MLV Reverse Transcriptase 5x reaction buffer (Promega, #M531A, USA), M-MLV Reverse Transcriptase (Promega, #M1701, Madison, USA), recombinant Ribonuclease Inhibitor (Promega, #N2511, Madison, USA), and recombinant dNTP Mix (Thermo Fisher Sientific, #R1092, Lithuania) were mixed with the sample and incubated at 37 °C for 1 h for reverse transcription. Quantitative RT-PCR (qRT-PCR) was performed in 96 well plates (FrameStar, 96 well plate #4ti-0770/C, UK) with DNA-DYE (GoTaq® qPCR Master Mix, #A600A, Madison, USA or Platinum™ Quantitative PCR SuperMix-UDG w/ROX, #11743500, Netherlands) using a 7500 Real-Time PCR System (Applied Bioscience) as previously described (12). The Primers were designed with Primer Express Software and are listed in supplemental table 1. Gene expression was calculated based on the ΔΔCt-method, and expressed as fold induction of mRNA expression. The housekeeping gene β-actin was used to normalize genes of interest.

Gel electroporation of PCR products

1.5 % agarose (Biozym, # 850471, Austria) gel was prepared with 8 µl DNA staining solution (Midori Green Advance, #MG04, Nippon Genetics, Japan). Final product of the qRT-PCR after 40 cycle of expansion for different genes (*Sftpc*, *Aqp5* and β-actin) from the hAEC, A549 and hSMA were loaded on the gel. Electrophoresis was performed at 120 V for 1 h. Gel was then transfer to UV imager (Biometra, # 032-001,302,303, Germany) and Image was taken to determine the DNA products.

Quantitative lung histomorphometric analysis

Lungs were inflated by pressure fixation at a constant pressure of 20 cm H_2O using fixative agent [4 % (mass/volume) of PFA] for 15 min. For PFA fixation, lungs were left in fixative for 30 min at RT and then stored in fixative agent at 4°C overnight. Next day, lungs were embedded in paraffin using automatic tissue embedder. For Isotropic Uniform Random (IUR) orientation, paraffin-embedded lungs were cut at random angles in 2 perpendicular planes

using a random number chart to select the angles. The paraffin blocks were re-mounted on blocks for sectioning. A random number from 1 to 100 defined how many 3 μm slices from the edge of the lung tissue were discarded to determine the start of the first series. Subsequently, series of thirty 3 μm sections were generated every 200 μm, and the lung sections were mounted on poly-l-lysine-coated glass slides. Randomly, four tissue sections were selected and deparaffinized using NeoClear rank (NeoClear, #1098435000, Merck, Darmstadt, Germany), and rehydrated in a gradual series of ethanol (100 %, 96 %, and 70 %, and finally PBS or destilled water). Next, tissue sections were stained with hematoxylin for 6 min, washed with distilled water and rinsed in regular tap water for 6 min. Afterwards, tissue was exposed to eosin for 5 min, followed by tissue dehydration in gradual series of ethanol (70 %, 80 %, 96 %, and 100 %, and Neo Clear), and finally tissue mounting using Neo-Mount® (Merck, # 109016, Germany). Images of lung sections were taken using a slide scanner (Leica SCN400 Slide Scanner, Houston, USA); up to ten fields of view per lung section (20x) were used for further analyses. We studied four randomly selected slides per animal and a total of five to six animals per group. Images were not taken in account when airways and vessels covered more than 15 % of the total area; atelectatic or not well inflated lungs were avoided.

Radial alveolar count: The radial alveolar count (RAC) method was described by Emery and Mithal, and used to count the number of alveoli across a terminal bronchus (13). Briefly, a line was drawn from terminal bronchiole to the nearest interlobular septum, and the number of distal air spaces the line crossed was counted.

Alveolar surface area: ImageJ-win64 (NIH, USA) was used to measure the alveolar surface area (ASA). Up to ten fields of view per lung section were selected for ASA; in each field of view up to ten random alveoli were selected and the alveolar diameter was measured. The alveolar diameter was used to calculate the surface area of an alveolus [4 *(pi) * r^2].

Alveolar septal thickness: As described previously (11), up to ten random alveoli per field of view were selected. The distance from the inner to the outer surface of the alveolar septum was measured to determine the septal thickness.

Mean Liner Intercept: Cell D 3.4 Olympus soft image solutions (Olympus, Hamburg, Germany) was used to determine the mean linear intercept (MLI). As described previously (1, 11), a grid of lines was used and each intercept of the lines and alveolar walls was counted and the total number of intercepts per field was divided through the total length of lines.

Elastic fibre quantification: Lung sections were stained for elastic fibers (purple) using Resorcin Fuchsin from Weigert (Weigert's Iron Resorcin and Fuchsin Solution; Carl Roth, X877.3) and counterstained yellow with Tartrazine [0.5 % in 0.25 % acetic acid (Dianova, cat. no. TZQ999, USA)]. The color thresholds were set to differentiate between elastic fibers and lung tissue. Elastic fiber density as an index of parenchymal elastin content was analyzed in up to ten fields of view per tissue section and four random tissue sections per animal (five to seven animals per group). Elastic fiber density of alveoli was measured using Cell D 3.4 Olympus Soft Imaging Solutions (Olympus; CellSens, Germany). First, the positive-stained area was defined manually as elastic fibers; next, an automatic quantification of the total elastic fiber-positive area was performed and related to the total area of tissue on the slide. The amount of elastic fibers relative to the total tissue served as a surrogate parameter for elastic fiber density. Areas where lung tissue was not well inflated or airway and/or blood vessel covered more than 15 % of the tissue area were excluded from the analysis. All images for calculation were taken at 40x magnification using a bright field microscope (Olympus, Hamburg, Germany).

Immunostaining

Tissue sections were deparaffinized and rehydrated as mentioned previously, then treated with MaxBlock™ reagent A (MaxVision Biosciences, #MB-L,Washington, USA) for 5 min at RT, and washed with 96 % ethanol and PBS. Antigen retrieval was performed by boiling

with 10 mM citrate buffer (pH 6; Dako, #S2369, Germany) at 90 - 120 °C for 25 min. Afterwards, tissue sections were incubated with blocking solution (Sea Block, Thermo Scientific™, #37527, Netherlands) at RT for 1 h. The incubation with the primary antibody mouse anti-αSMA-CY3 (Sigma-Aldrich, #C6198, USA, 1:200) was performed in the dark at 4 °C overnight. Sections were then washed with PBS and treated with DAPI dye (Sigma-Aldrich, #D9542, Germany, 1:5000) to counterstain the nucleus. Lung tissue sections were incubated with Post-Detection Conditioner Reagent B (MaxVision Biosciences, #MB-L, Washington, USA) for 5 min at RT to enhance the fluorescent signal, and then mounted in fluoromount aqueous (Sigma Aldrich, #F4680, USA). Images of lung sections were taken using a fluorescence microscope (Olympus, Hamburg, Germany) at 40x and 100x magnification. These images were used to count αSMA^+ cells in four fields of view in two random sections per animal (four animals per group).

TUNEL and SFTPC staining

Tissue section and Precision-Cut Lung Slices (PCLS) were treated with MaxBlock™ reagent A (MaxVision Biosciences, #MB-L,Washington, USA) for 5 min at RT and washed with 60 % ethanol and PBS. Antigen retrieval was performed by treating the sections with proteinase K solution (Thermo Scientific™, #EO0491, Lithuania) for 15 min at 37°C. The tissue sections were then incubated with blocking solution (Sea Block, Thermo Scientific™, #37527, Netherlands). Subsequently, the lung sections were exposed to terminal uridine deoxynucleotidyl transferase dUTP terminal nick end labeling (TUNEL) solution according to the manufacturer's instructions (*In Situ* Cell Death Detection Kit, Roche, #11684795910, Germany) for 1 h at 37 °C. Next, the sections were washed with PBS-T and then incubated with rabbit anti-pro-SFTPC antibody (Merck, #AB3786, Germany, 1:200) in dark at 4 °C overnight. The following day, the sections were washed with PBS-T and treated with secondary antibody conjugated with CY3 (Dianova, #111-165-003, USA) for 1 h at RT; cell nuclei were stained with DAPI (Sigma-Aldrich, #D9542, Germany). Finally, the tissue

sections were mounted (Fluoromount™ Aqueous Mounting Medium, Sigma-Aldrich, #F4680, USA) and images were taken directly at 40x and 100x magnification using a fluorescence microscope (Olympus, Hamburg, Germany). These images were used to calculate the total $TUNEL^+$, $SFTPC^+$ and $TUNEL^+/SFTPC^+$ cells in four fields of view in one or two random sections per animal (four animals per group for *in vivo* studies and three to four animals per group for PCLS).

Precision Cut Lung Slices (PCLS):

Murine lungs were isolated from 14-days old mice after intratracheal instillation of agarose (2 % agarose in HBSS). Lungs were sliced with a thickness of 200 µm and cultured with serum-rich medium [Dulbecco's Modified Eagle Medium, Gibco, #41966-029, Netherlands) supplemented with 10 % FBS and 1 % Penicillin/Streptomycin (P/S)] for 24 h. The lung sections were then treated with 100 ng of IL-6 (Sigma-Aldrich, #I9646, Germany) + 20 ng IL-6Ra (IL-6Ra Protein, R&D Systems, #1830-SR-025, USA) (IL-6/sIL-6R), or vehicle (0.1 % BSA) and exposed to either normoxia (21 % O_2, NOX) or hyperoxia (85 % O_2, HYX) for 48 h, followed by fixation of the PCLS with 4 % PFA and paraffin-embedding. Subsequently, sections of 3 µm thickness were produced and immunofluorescence staining for SFTPC (Merck, #AB3786, Germany) was combined with TUNEL detection (*in situ* Cell Death Detection Kit, Roche, #11684795910, Germany). The total number of $TUNEL^+$ cells as well as the number of $TUNEL^+$ and $SFTPC^+$ cells (double-positive) were counted from 4 different areas per lung section; lungs of 3-5 different mice were used.

Cell culture experiments

Mouse Lung Epithelial cells

Mouse Lung Epithelial cells (MLE12; ATCC, CRL-2110; Manassas, VA) were cultured according to the ATCC recommendations in Dulbecco's medium, Ham's F12 (DMEM/F12)

(Gibco, #11039-021, Netherlands) supplemented with fetal bovine serum (FBS; Merck, #S0615, Germany), hydrocortisone (Sigma, #H6909; St Louis, MO), insulin-transferrin-selenit-X-supplement (Gibco™, #51500-056, Netherlands), β-estradiol (Sigma, #E2758, Germany) and Penicillin/Streptomycin solution (P/S; Sigma-Aldrich, #P4458-100ML, Germany). Cells (passage 2-10) were subcultured every 3-4 days at a 1:8 ratio. MLE12 cells were grown in 6-well plates and 96-well plates to 80 % confluency in a medium with 2 % FBS (FBS-rich medium) and starved overnight for 12 h in a medium with 0.2 % FBS (FBS-reduced medium). Subsequently, MLE12 cells were treated 1) for 24 h at either normoxia or hyperoxia with 100 ng IL-6 (Sigma-Aldrich, #I9646, Germany) + 20 ng IL-6Ra (IL-6Ra Protein, R&D Systems, #1830-SR-025, USA) (IL-6/sIL-6R), 2) for 24 h with conditioned media (secretome, supernatant) from macrophages, which were exposed to normoxia (21 % O_2) or hyperoxia (85 % O_2) or 3) the respective vehicles. BSA (0.1%) served as vehicle for IL-6/sIL-6R. At the end of the experiment, cell viability was assessed using MTT-assay or mRNA was extracted.

Primary human alveolar epithelial cells (hAEC)

Primary human alveolar epithelial cells (PELOBiotech, #PB-H-6053, Germany) were cultured according to the recommendations in medium provided by PELOBiotech (CellBiologics; PELOBiotech; #PB-H6621). 10.000 hAECs per well were seeded in a 96 well plate and allowed to grow for 24 h. Subsequently, hAECs were treated 1) for 24 h under normoxia (21 % O_2) or hyperoxia (85 % O_2) with 100 ng IL-6 (Sigma-Aldrich, # I1395, Germany) + 20 ng IL-6Ra (IL-6Ra Protein, R&D Systems, #227-SR, USA) (IL-6/sIL-6R), 2) for 24 h with conditioned media (secretome, supernatant) from human macrophages of three different donors (M0-like and M1-like), which were exposed to normoxia (21 % O_2) or hyperoxia (85 % O_2) for 48 h, or 3) the respective vehicles. BSA (0.1%) served as vehicle for IL-6/sIL-6R. At the end of the experiment, cell proliferation was assessed using MTT-assay (ATCC; #30-1010K).

A549 cells

Human lung carcinoma cell line (A549) (ATCC, #CCL-185™, USA) cells were cultured with DMEM/F12 (Dulbecco's Modified Eagle Medium/F12, Gibco, #11320-033, Netherlands) supplemented with 10 % FBS (serum-rich medium) and 1 % Penicillin/Streptomycin (P/S) according to the recommendation of ATCC. Cells were grown at on glass slides and in T75 flask at 37 °C and 5 % CO_2. When cells were 80 % confluent, cells were used for immunostaining and mRNA isolation.

Primary human bronchial smooth muscle cells (hSMC)

Human bronchial smooth muscle cells (hSMC) (PromoCell, #C-12561, Heidelberg, Germany) and grown according to the recommendations (PromoCell; Smooth Muscle Cell Growth Medium 2: Lot#427M002; Supplement-Mix: Lot#425M235, Heidelberg, Germany) at 37 °C and 5 % CO_2. When cells were 80 % confluent, cells were used for mRNA isolation.

Macrophages

Mouse ascites macrophages (J774.A1, ATCC® TIB-67™) cells were cultured with DMEM (Dulbecco's Modified Eagle Medium, Gibco, #41966-029, Netherlands) supplemented with 10 % FBS (serum-rich medium) and 1% Penicillin/Streptomycin (P/S) according to the recommendation of ATCC. Cells were grown on plates (Falcon®, #353003, USA) at 37 °C, 5 % CO_2. When cells were 80 % confluent, media was changed to DMEM with 1 % FBS (serum-reduced medium) and exposed to either normoxia or hyperoxia for 48 h. At the end of the experiment, the supernatant (conditioned media; secretome of the macrophages) was collected for ELISA or for treatment of MLE12 cells, and macrophages were harvested for further analyses.

Primary murine macrophages

Isolation of peritoneal macrophages was performed as described previously (14). Briefly, WT C56BL/6J mice received an intraperitoneal injection of 1 ml Brewer's thioglycolate medium (BD-BBL™, #221195, USA) and were sacrificed four days after. A peritoneal lavage of 5 times 5 ml of serum-free medium (Dulbecco's Modified Eagle Medium, Gibco, #41966-029, Netherlands) was performed. Macrophages from the peritoneal cavity were centrifuged at 1500 rpm or 300 g for 10 min at 4°C. The cell pellets were resuspended in 1 ml of serum-rich medium. 500.000 macrophages per well were seeded in a 6-well plate and cultured with serum-reduced medium (1% FBS) under normoxia (21 % O_2) or hyperoxia (85 % O_2) for 48 h. At the end of the experiments, the conditioned medium was collected to treat hAEC; mRNA was isolated from macrophages and gene expression was assessed.

Human monocyte-derived macrophages and differentiation

Human blood was collected from the hospital blood bank (for ethical consent see below).

M0 Macrophages

Human macrophages were generated from peripheral blood mononuclear cells (PBMCs) as previously described (15, 16). Briefly, PBMCs were isolated from buffy coats obtained from the blood bank of the Universities of Giessen and Marburg Lung Center (AZ 58/15) using Ficoll density gradient centrifugation. Platelets and red blood cells (RBC) were removed by two washing steps with RBC lysis buffer (BD Biosciences) and phosphate-buffered saline (PBS), respectively. Finally, monocytes were differentiated to macrophages during 10 days in RPMI containing 2.5% human serum, 4 mML-glutamine, and penicillin/streptomycin in six-well tissue culture plates. Next, we exposed M0 macrophages to normoxia (21 % O_2) or hyperoxia (85 % O_2) for 48 h. At the end of the experiments, the conditioned medium was

collected to treat hAEC; mRNA was isolated from macrophages and gene expression was assessed.

M1 Macrophages

Isolation of monocyte-derived macrophages was performed as described previously (17). Buffy coat from the blood was collected from the hospital blood bank of the University Hospital Cologne (approval No 06.062) and treated with the magnetic beads-containing antibody against CD14 cell marker (Miltenyi Biotec #130-110-520, Germany). $CD14^+$ cells were collected and kept in serum-rich medium [Roswell Park Memorial Institute (RPMI) Medium, Gibco, #RPMI1640) supplemented with 10 % FBS and 1 % Penicillin/Streptomycin (P/S)]. For differentiation in M1-like monocyte-derived macrophages, $CD14^+$ cells were treated with Granulocyte-macrophage colony-stimulating factor (GM-CSF; 100 ng/ml) for 7 days in serum-rich medium; the media was changed on alternate days. After 7 days, monocyte-derived macrophages were cultured with GM-CSF in serum-reduced (1 % FBS) medium and exposed to normoxia (21 % O_2) or hyperoxia (85 % O_2) for 48 h. At the end of the experiments, the conditioned medium was collected to treat hAEC; mRNA was isolated from macrophages and gene expression was assessed.

Immunocytochemistry of hAEC, A549, and hSMC

Cells (hAEC, A549 and hSMA) were cultured overnight on glass slides that were coated with 0.2 % gelatin (30 min at 37°C). Cells were then fixed with pre-cooled methanol for 5 min , subsequently washed with PBS, and treated with blocking solution for 1 h. Primary antibody for rabbit anti-pro-surfactant protein C (SFPTC; Merck, #AB3786, Germany, 1:200) and rabbit anti-Aquaporin 5 (AQP5; Sigma-aldrich, #A4979-200UL, Germany, 1:200) were applied for overnight. Next day, cells were washed with PBS and treated with secondary antibody conjugated with CY3 (Dianova, #111-165-003, USA) and Alexa (Jacksonimmuno, #111-485-003, USA) for 1 h at RT. Cell nuclei were stained with DAPI (Sigma-Aldrich, #D9542, Germany). Finally, cells were mounted (Fluoromount™

Aqueous Mounting Medium, Sigma-Aldrich, #F4680, USA) and images were taken directly at 100x magnification using a fluorescence microscope (Olympus, Hamburg, Germany).

IL-6 ELISA: Conditioned media of macrophages was used for ELISA to determine the IL-6 concentration. ELISA was performed according to the manufacturer's guidance (IL-6 Mouse Uncoated ELISA Kit, Invitrogen, #88-7064-22, USA). In brief, ELISA plate was incubated with IL-6 capture antibody overnight at 4 °C, followed by adding 100 µl sample (conditioned media) per well and incubated for 2 h at RT. The plate was then washed with washing buffer, 100 µl of detection antibody was added to each well and incubated at RT for 1 h. Next, 100 µl of avidin-HRP conjugated antibody was added to the plate and incubated for 30 min at RT. Afterwards incubation with 100 µl of TMB solution (substrate for avidin-HRP) was performed for 15 min; the reaction was stopped by adding the stop solution (2N H_2SO_4). Finally, the optical density (OD) was measured at 450/570nm (Tecan Infinite® 200 PRO, Switzerland).

MTT assay: MTT assay was performed according to the guidelines of the manufacturer (ATCC, #30-1010K, USA). To this end, 10.000 MLE12 cells were incubated in a 96 well plate for 24 h, followed by 12 h starvation with serum-reduced medium. Cells were then washed with PBS, and serum-reduced MLE12 medium and conditioned media of macrophages were added to each well (1:1 ratio). For control, serum-reduced MLE12 medium a well as DMEM with 1% FBS (medium used for macrophages) was used (1:1 ratio). Cells were exposed to either normoxia (21 % O_2) or hyperoxia (85 % O_2) for 24 h. Afterwards, cells were incubated with 10 µl of tetrazolium dye MTT 3-(4,5-dimethylthiazol-2-yl)-2,5-diphenyltetrazolium bromide for 2 h, and treated with 100 µl of detergent provided by the manufacturer for 2 h. Absorbance was measured at 570 nm (Tecan Infinite® 200 PRO, Switzerland).

si-Klf4 transfection in macrophages: Cultured J774.a1 were transfected with either anti Klf4-siRNA (si-klf4; Dharmacon, Cat. No. SO-2589106G, USA) or scrambled siRNA (scr-siRNA; Dharmacon, Cat. No. SO-2588425G, USA) using Endo-Porter (GeneTools LLC, Philomath, Oregon, USA). Briefly, macrophages were grown to 70 % confluency in serum-rich medium, followed by transfection of 20 ng si-klf4 or scr-klf4 at 37 °C and 5 % CO_2 for 24 h using the following medium: 6 µl of 1 mM Endo-Porter (GeneTools LLC, Philomath, Oregon, USA) in 1 ml of antibiotic free complete media (DMEM with 10 % FBS). Afterwards, the media was changed and the transfected cells were maintained in serum-rich medium for 24 h. Finally, cells were starved with serum-reduced medium for 12 h, followed by exposure to either normoxia or hyperoxia for 48 h. At the end of the experiments, macrophages were harvested for further analysis.

Human lung tissue

BPD and control (non-diseased) postnatal human lung tissues were obtained through the NHLBI LungMAP Consortium Human Tissue Core Biorepository (BRINDL) through the work of the U.S. Transplantation program, the International Institute for the Advancement of Medicine and the National Disease Research Interchange. The Biorepository is approved by the University of Rochester Research Subjects Review Board (RSRB00056775). Consent for research use has been provided for each sample. Clinical metadata and histopathology was assessed in each case to determine a combined diagnosis based on clinical history and pathology of the lung tissue (ClinPathDx, Table 1).

Immunostaining of human lungs

Paraffin embedded BPD and control (non-diseased) postnatal human lungs were sectioned at 5 µm, deparaffinized with xylene, rehydrated in decreasing graded ethanol concentrations, and boiled in a sodium citrate antigen retrieval solution (10 mM, pH 6.0) for 12 min. Slides were then washed in TBST (TBS and 0.1 % Tween). Endogenous peroxidase was quenched 3

% H_2O_2 for 15 min. Slides were then washed in TBST and blocked using 3 % bovine serum albumin/5 % Normal Goat Sera/0.1 % Triton (serum type was dependent on the secondary antibodies being used) for at least 1 h at RT. Slides were incubated with the following primary antibodies overnight at 4 °C: pSTAT3 (Cell Signaling, #9145, 1:200), CD45 (Invitrogen, #14-9457-82; 1:200), CDH1 (BD Biosciences, 610181; 1:200), CD68 (eBioscience, 14-0688-82; 1:200, San Diego, USA), and Surfactant protein C (SFTPC, LSBio,LS-B10952; 1:100, Seattle, USA). The following day slides were washed with TBST and incubated for 1 h at RT with appropriate Cy-3 and Cy5-conjugated secondary antibodies (Jackson Immunoresearch Laboratories, Inc., West Grove, PA, USA). Slides were then stained for DAPI (DE571; LifeTechnologies, Carlsbad, USA) and mounted using ProLong Diamond Antifade Mountant (LifeTechnologies, Carlsbad, USA).

In Situ Hybridization of Human Lungs

Fluorescent *in situ* hybridization was conducted using the Advanced Cell Diagnostics RNAscope Fluorescent Multiplex Assay following the manufacturer's instructions, with minor adjustments. Treatment time with Protease Plus was decreased to 22 min. Tissue was incubated with *IL6* probe (Advanced Cell Diagnostics; 310371) for 2 h at 40 °C on protocol day 1, followed by washing in RNAscope wash buffer, and stored overnight at RT in 5X SSC. On day 2 the protocol was continued as described in the manual until the HRP blocker step was completed. Slides were then washed with RNAscope wash buffer and proceeded onto CDH1 immunofluorescent staining. Slides were blocked using 3 % bovine serum album/5 % Normal Goat Sera/0.1 % Triton for at least 1 h at RT, and incubated overnight at 4 °C with primary antibody CDH1 (BD Biosciences, 610181, 1:200). The following day slides were washed with TBST and incubated for 1 h at RT with Cy5-goat-anti-mouse-conjugated secondary antibody (Jackson Immunoresearch Laboratories, Inc., West Grove, PA, USA). Slides were then stained for DAPI (DE571; LifeTechnologies) and mounted using ProLong Diamond Antifade Mountant (LifeTechnologies).

Human cohort study Stanford

Premature infants who were born at ≤ 32 weeks gestational age (GA) and admitted to the neonatal intensive care unit (NICU) at Lucile Packard Children's Hospital Stanford were prospectively enrolled into a longitudinal study designed to assess clinical biomarkers of BPD. We have previously reported on this cohort(10). Infants with complex congenital heart disease, inherited metabolic disorders and/or lethal congenital malformations were excluded from participation. Plasma specimens were obtained at weekly time points during their hospitalization, and clinical characteristics were abstracted from their medical records. Infants were followed to 36 weeks post-conceptual age (PCA) to determine if they acquired BPD based on NIH criteria, defined by the ongoing need for either supplemental O_2 and/or positive pressure respiratory support. The study was approved by the Stanford University Institutional Review Board (Protocol #20210). Supplemental table 2 shows maternal and infant characteristics at birth for infants enrolled in the study. Plasma specimens were dispensed into 50 µl aliquots that were immediately frozen at -80 °C for later batch processing. Plasma was assayed for cytokine profiling via the Human Immune Monitoring Center at Stanford University using a validated custom-built Human 63-plex bead assay (eBiosciences/Affymetrix).

References:

1. Alejandre-Alcazar MA, Kwapiszewska G, Reiss I, Amarie OV, Marsh LM, Sevilla-Perez J, Wygrecka M, Eul B, Kobrich S, Hesse M, Schermuly RT, Seeger W, Eickelberg O, Morty RE. Hyperoxia modulates TGF-beta/BMP signaling in a mouse model of bronchopulmonary dysplasia. *Am J Physiol Lung Cell Mol Physiol* 2007; 292: L537-549.
2. Barkhausen T, Tschernig T, Rosenstiel P, van Griensven M, Vonberg RP, Dorsch M, Mueller-Heine A, Chalaris A, Scheller J, Rose-John S, Seegert D, Krettek C, Waetzig GH. Selective blockade of interleukin-6 trans-signaling improves survival in a murine polymicrobial sepsis model. *Crit Care Med* 2011; 39: 1407-1413.
3. Li ZW, Omori SA, Labuda T, Karin M, Rickert RC. IKK beta is required for peripheral B cell survival and proliferation. *J Immunol* 2003; 170: 4630-4637.
4. Claxton S, Kostourou V, Jadeja S, Chambon P, Hodivala-Dilke K, Fruttiger M. Efficient, inducible Cre-recombinase activation in vascular endothelium. *Genesis* 2008; 46: 74-80.
5. Langmead B, Salzberg SL. Fast gapped-read alignment with Bowtie 2. *Nat Methods* 2012; 9: 357-359.
6. Li B, Dewey CN. RSEM: accurate transcript quantification from RNA-Seq data with or without a reference genome. *BMC Bioinformatics* 2011; 12: 323.
7. Robinson MD, McCarthy DJ, Smyth GK. edgeR: a Bioconductor package for differential expression analysis of digital gene expression data. *Bioinformatics* 2010; 26: 139-140.
8. Dinger K, Kasper P, Hucklenbruch-Rother E, Vohlen C, Jobst E, Janoschek R, Bae-Gartz I, van Koningsbruggen-Rietschel S, Plank C, Dotsch J, Alejandre Alcazar MA. Early-onset obesity dysregulates pulmonary adipocytokine/insulin signaling and induces asthma-like disease in mice. *Sci Rep* 2016; 6: 24168.
9. Dinger K, Mohr J, Vohlen C, Hirani D, Hucklenbruch-Rother E, Ensenauer R, Dotsch J, Alejandre Alcazar MA. Intraperitoneal Glucose Tolerance Test, Measurement of Lung Function, and Fixation of the Lung to Study the Impact of Obesity and Impaired Metabolism on Pulmonary Outcomes. *J Vis Exp* 2018.
10. Alejandre Alcazar MA, Kaschwich M, Ertsey R, Preuss S, Milla C, Mujahid S, Masumi J, Khan S, Mokres LM, Tian L, Mohr J, Hirani DV, Rabinovitch M, Bland RD. Elafin treatment rescues EGFR-Klf4 signaling and lung cell survival in ventilated newborn mice. *Am J Respir Cell Mol Biol* 2018.
11. Will JP, Hirani DV, Thielen F, Klein F, Vohlen C, Dinger K, Dotsch J, Alejandre-Alcazar MA. Strain-dependent effects on lung structure, matrix remodeling and Stat3/Smad2 signaling in C57BL/6N and C57BL/6J mice after neonatal hyperoxia. *Am J Physiol Regul Integr Comp Physiol* 2019.
12. Mohr J, Voggel J, Vohlen C, Dinger K, Dafinger C, Fink G, Gobel H, Liebau MC, Dotsch J, Alejandre Alcazar MA. IL-6/Smad2 signaling mediates acute kidney injury and regeneration in a murine model of neonatal hyperoxia. *FASEB J* 2019: fj201801875RR.
13. Emery JL, Mithal A. The number of alveoli in the terminal respiratory unit of man during late intrauterine life and childhood. *Arch Dis Child* 1960; 35: 544-547.
14. Gonc¸alves, R. and Mosser, D.M. 2015. The isolation and characterization of murine macrophages. *Curr. Protoc. Immunol.* 2015 111:14.1.1-14.1.16..
15. Pullamsetti SS, Kojonazarov B, Storn S, Gall H, Salazar Y, Wolf J, Weigert A, El-Nikhely N, Ghofrani HA, Krombach GA, Fink L, Gattenlöhner S, Rapp UR, Schermuly RT, Grimminger F, Seeger W, Savai R. Lung cancer-associated pulmonary hypertension: Role of microenvironmental inflammation based on tumor cell-immune cell cross-talk. *Sci Transl Med.* 2017 Nov 15;9(416):eaai9048.
16. Sarode P, Zheng X, Giotopoulou GA, Weigert A, Kuenne C, Günther S, Friedrich A, Gattenlöhner S, Stiewe T, Brüne B, Grimminger F, Stathopoulos GT, Pullamsetti SS, Seeger W, Savai R. Reprogramming of tumor-associated macrophages by targeting β-catenin/FOSL2/ARID5A signaling: A potential treatment of lung cancer. *Sci Adv.* 2020 Jun 5;6(23):eaaz6105.
17. Izquierdo E, Cuevas VD, Fernández-Arroyo S, Riera-Borrull M, Orta-Zavalza E, Joven J, Rial E, Corbi AL, Escribese MM. Reshaping of Human Macrophage Polarization through Modulation of Glucose Catabolic Pathways. *J Immunol*. 2015 Sep 1;195(5):2442-51.

Supplementary Table 1

Gene	Species m = mouse h = human	Primer	Sequence
αsma *(Acta2)*	m	for	ACATCAGGGAGTAATGGTTGGAAT
		rev	GGTGCCAGATCTTTTCCATGTC
		probe	CGATAGAACACGGCATCATCACCAACTG
Arg1	m	for	ACCCTGACCTATGTGTCATTTGG
		rev	TGGTACATCTGGGAACTTTCCTTT
		probe	ATGCTCACACTGACATCAACACTCCCCTG
Aqp5	m	for	TCACTGGGTCTTCTGGGTAGGA
		rev	CTGGCTCATATGTGCCTTTGAC
		probe	TACTTCTACTTGCTTTTCCCCTCCTCGCTG
**Aqp5*	h	for	CCACCTTGTCGGAATCTACTTCA
		rev	GGGCCCTACCCAGAAAACC
βactin	m	for	TGACAGGATGCAGAAGGAGATTACT
		rev	GCCACCGATCCACACAGAGT
		probe	ATCAAGATCATTGCTCCTCCTGAGCGC
**βactin*	h	for	GATGGCCACGGCTGCTT
		rev	ACCCTCATTGCCAATGGT
Ccl2	m	for	GGCTCAGCCAGATGCAGTTAAC
		rev	CTTGGTGACAAAAACTACAGCTTCTT
		probe	CCCCACTCACCTGCTGCTACTCATTCA
Ccl7	m	for	TGGGAAGCTGTTATCTTCAAGACA
		rev	TTCTGTTCAGGCACATTTCTTCA
		probe	CTTAGACATGAAAACCCCAACTCCAAAGCC
**Col1a1*	m	for	GCAGTGCTGTTGCGATCTTG
		rev	CAGAGGGACAGAGCACAGCTT
Cxcl5	m	for	TGGCATTTCTGTTGCTGTTCA
		rev	GCTCCGTTGCGGCTATGA
		probe	AGCATCTAGCTGAAGCTGCCCCTTCCT
**Fbn1*	m	for	GGTCAATGCAACGATCGAAA
		rev	AGTGTGACAAAGGCAGTAGAAGCTT
**Fbln5*	m	for	TACATCCTACTCAGGCCCATACC
		rev	GTTGCCTTCATCCATCTGATACC
Fizz1	m	for	CGTGGAGAATAAGGTCAAGGAACT
		rev	CACTAGTGCAAGAGAGAGTCTTCGTT
		probe	TTGCCAATCCAGCTAACTATCCCTCCACTG
**IL1b*	h	for	CTAAACAGATGAAGTGCTCC
		rev	GGTCATTCTCCTGGAAGG
**Il4*	m	for	GGAGATGGATGTGCCAAACG
		rev	GCACCTTGGAAGCCCTACAG
Il6	m	for	ACAAGTCGGAGGCTTAATTACACAT
		rev	AATCAGAATTGCCATTGCACAA
		probe	TCTTTTCTCATTTCCACGATTTCCCAGAGAA
**IL6*	h	for	GTACATCCTCGACGGCATCTC
		rev	GCTGCTTTCACACATGTTACTCTTG

Il17a	m	for	CCAGAAGGCCCTCAGACTACCT
		rev	GGGATATCTATCAGGGTCTTCATTG
		probe	AACCGTTCCACGTCACCCTGGACTC
Mmp12	m	for	GCAGCAGTTCTTTGGGCTAGA
		rev	GTACATCGGGCACTCCACATC
		probe	CTGGGCAACTGGACAACTCAACTCTGG
**MMP12*	h	for	GTCCCTGTATGGAGACCCAAAA
		rev	ACGGTAGTGACAGCATCAAAACTC
**Sftpa*	m	for	TCAAACATCAGATTCTGCAAACAA
		rev	TGACTGCCCATTGGTGGAA
**Sftpb*	m	for	CTGCTGGCTTTGCAGAACTCT
		rev	GAGGACAAGGCCACAGACTAGCT
**Sftpc*	m	for	CCTCGTTGTCGTGGTGATTGTA
		rev	GCTCATCTCAAGGACCATCTCAGT
**Sftpc*	h	for	GCACCTGCTGCTACATCATGA
		rev	CCATCTGGAAGTTGTGGACTTTT
**Sftpd*	m	for	CAGCAGATGGAGGCCTTAAAA
		rev	GGGAACAATGCAGCTTTCTGA
Socs3	m	for	CCACCCTCCAGCATCTTTGT
		rev	TCCAGGAACTCCCGAATGG
		probe	ACTGTCAACGGCCACCTGGACTCCT
Tlr4	m	for	GGTGAGAAATGAGCTGGTAAAGAATT
		rev	GCAATGGCTACACCAGGAATAAA
		probe	TGCCCCGCTTTCACCTCTGCC
**TLR4*	h	for	CATTTCAGCTCTGCCTTCACTACA
		rev	ATGGAAACCTTCATGGATGATGT
**TNFa*	h	for	CCCAGGGACCTCTCTCTAATCAG
		rev	TCAGCTTGAGGGTTTGCTACAA

Supplementary table1. List of primers used for real-time RT-PCR; *SYBR-Green primer.

Supplementary Table 2

	Number (% of cohort)
Male / Female	37 (67 %) / 18 (33 %)
Race: White	37 (67 %)
Asian	12 (22 %)
Black	3 (5.5 %)
Pacific Islander	3 (5.5 %)
Hispanic ethnicity	24 (43 %)
Cesarean delivery	37 (67 %)
Multiple gestation	21 (38 %)
Vaginal bleeding	8 (14.5 %)
Placenta Previa	2
Abruptio Placenta	6
Maternal pre-eclampsia	17 (31 %)
Maternal prolonged rupture of membranes (PROM)	14 (25 %)
Intrauterine growth restriction (IUGR)	4 (7 %)
Antenatal corticosteroid treatment	36 (65 %)
Maternal group B streptococcal infection	4 (7 %)
APGAR at 1 minute (mean, SD)	5.6 (2.6)
APGAR at 5 minute (mean, SD)	7.6 (1.8)
Surfactant treatment	24 (43 %)
Bronchopulmonary dysplasia (BPD)	15 (27 %)
MV/CPAP (days, median & [range])[§]	2 [0-217]

nCPAP (days, median & [range])¶	17 [0-55)]
High-frequency ventilation treatment (n)	8
Days on respiratory support (mean ± SD)	61 ± 46
Days in hospital (mean ± SD)	86 ± 47
Patent ductus arteriosus (n)	16
Indomethacin treatment (n)	15
Caffeine treatment (n)	26

Supplementary table 2. Demographic and relevant clinical data for the infants enrolled, including maternal/pregnancy related data.

Supplementary Figure 1:

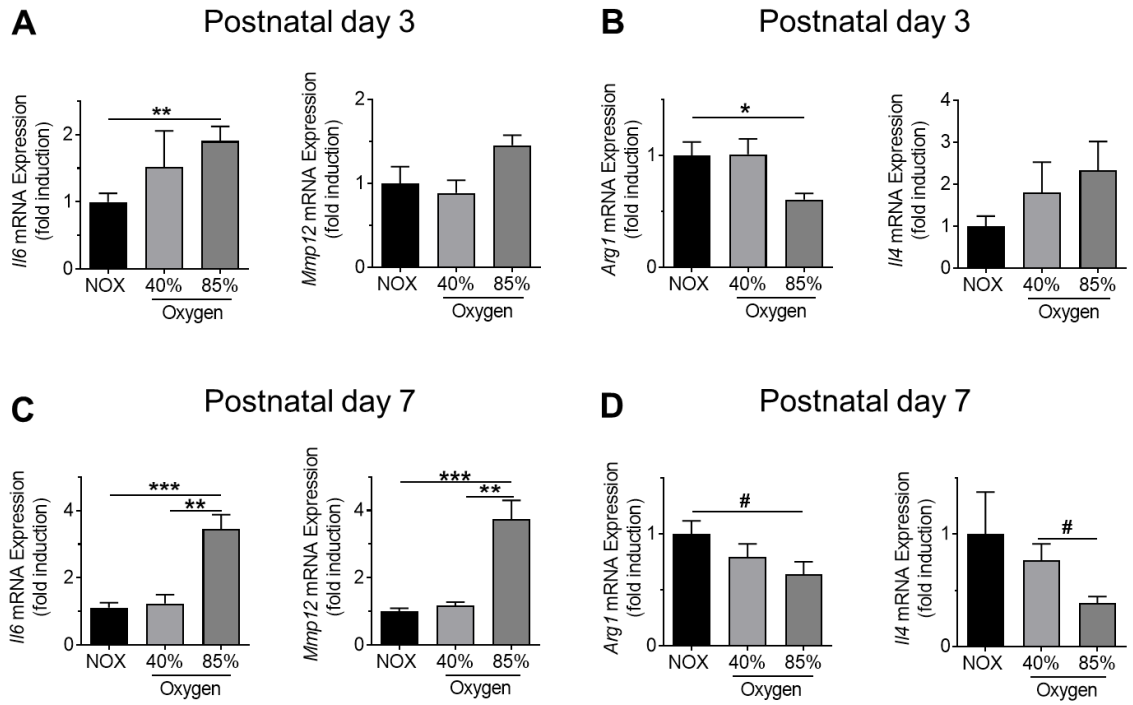

Supplementary Figure 1: *Effect of mild hyperoxia (40% O_2) and high hyperoxia (85% O_2) on gene expression of macrophage markers in mouse lungs at postnatal day 3 (P3) and P7.* Wildtype mice were exposed to 40 % O_2 or 85 % O_2 from birth until P3 or P7. A, C: Measurement of gene expression of M1-like markers in total lung homogenates at P3 (A) and P7 (C) using qRT-PCR; interleukin 6 (*Il6*) and metalloproteinase 12 (*Mmp12*); n=7 / group; β-actin served as housekeeping gene. B, D: Gene expression of M2-like markers in total lung homogenates at P3 (B) and P7 (D) using qRT-PCR: arginase 1 (*Arg1*) and interleukin 4 (*Il4*); n=7 / group. Mean±SEM; Kruskal-Wallis One-way ANOVA with Dunn's post-test: *p<0.05; **p<0.01; ***p<0.001; unpaired t-test: $^{\#}$p<0.05.

Supplementary Figure 2:

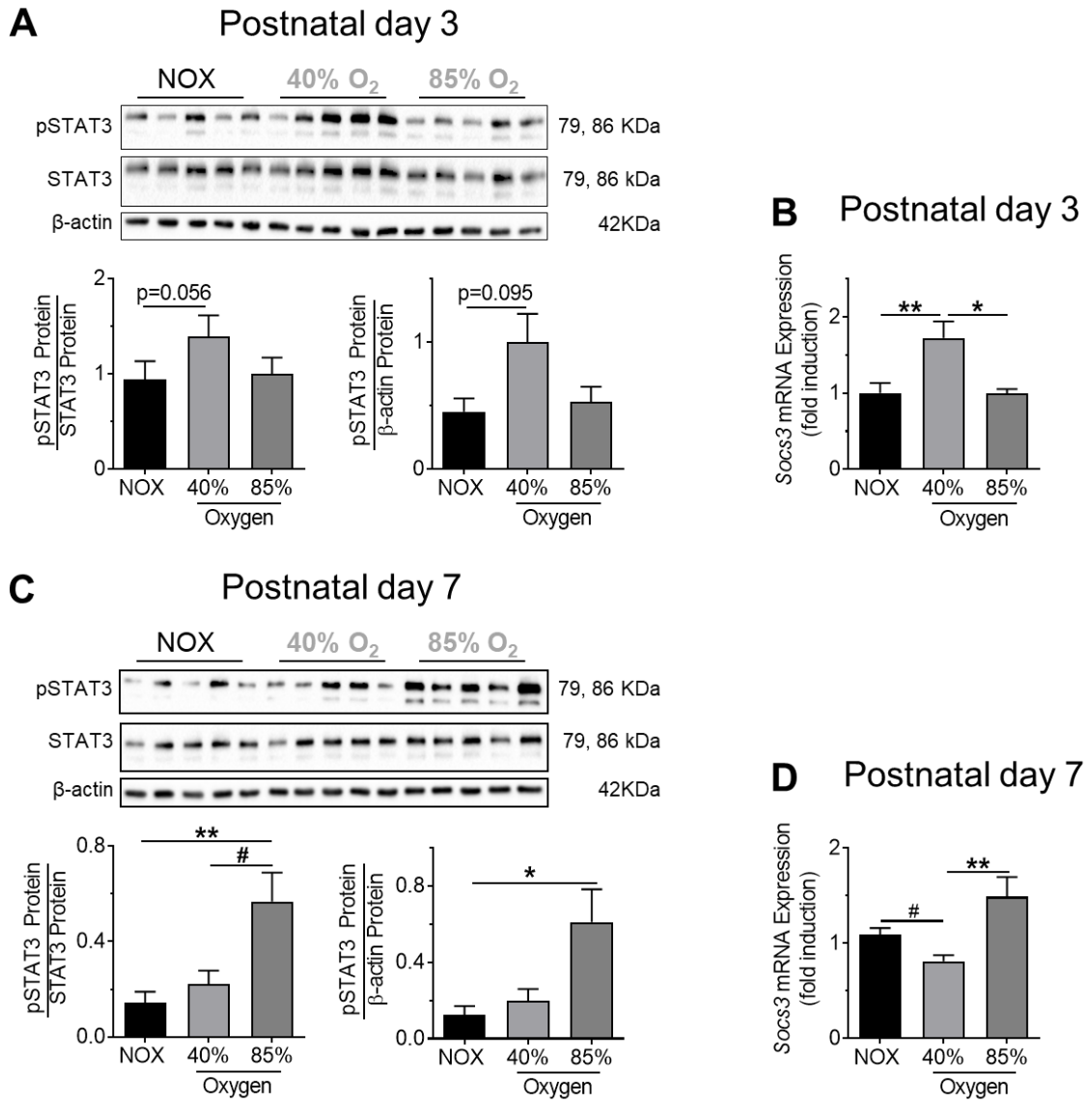

Supplementary Figure 2: *Effect of mild hyperoxia (40% O_2) and high hyperoxia (85% O_2) on activation of STAT3/SOCS3 signaling in mouse lungs at postnatal day 3 (P3) and P7.* Wildtype mice were exposed to 40% O_2 or 85% O_2 from birth until P3 or P7. A, C: Immunoblots showing phosphorylated STAT3 (pSTAT3), total STAT3 and β-actin protein abundance in total lung homogenates after exposure to Normoxia (NOX), 40% O_2 or 85% O_2; P3 (A), and P7 (C); pSTAT3 protein was related to STAT3 or β-Actin, which served as a loading control; densitometric data are displayed under the immunoblot; n = 5/group. B, D: Assessment of gene expression of suppressor of cytokine signaling 3 (*Socs3*) in total lung homogenates at P3 (B) and P7 (D); n=7-15/ group. Mean±SEM; Kruskal-Wallis One-way ANOVA with Dunn's post-test: *p<0.05; **p<0.01; Mann-Whitney test: $^{\#}$p<0.05.

Supplementary Figure 3:

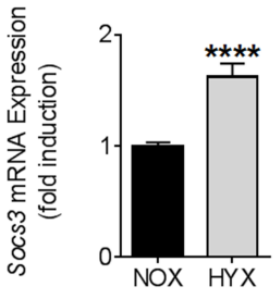

Supplementary Figure 3: Measurement of *Socs3* mRNA as IL-6/STAT3 target gene in lungs at P28 by qRT-PCR (n = 10-12/group); gene expression is shown as fold induction. Mean±SEM; non-parametric Mann-Whitney test: ****p<0.0001.

Supplementary Figure 4:

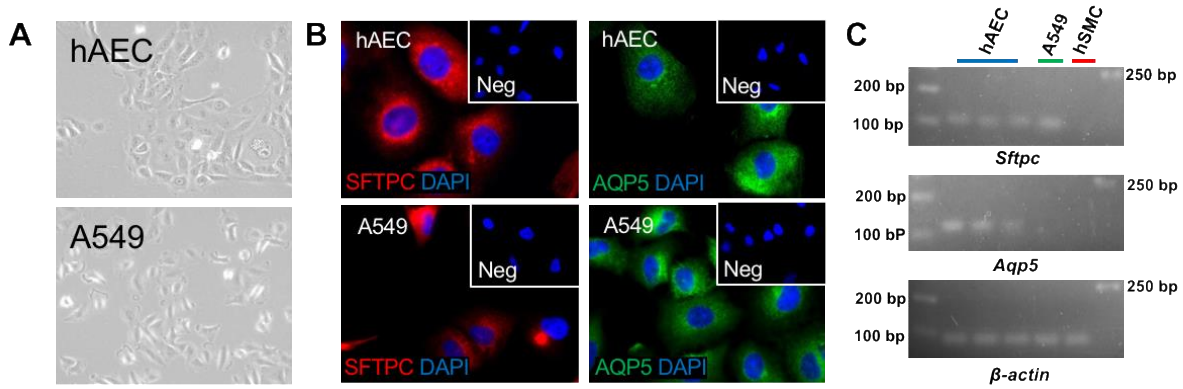

Supplementary Figure 4: (A): Morphological image of human alveolar epithelial cells (hAEC) and A549 cells. (B) Representative immunofluorescent staining for SFTPC (red) and AQP5 (green) in hAEC and A549, cultured for 24 h on glass slides, fixed with methanol, and subsequently stained. IgG antibody was used as negative control. (C) Gel electrophoresis of qRT-PCR products of *Sftpc*, *Apq5* and β-actin from hAEC, A549 and human bronchial smooth muscle cells (hSMC); the cells were cultured until they reached 80% of confluency and then harvested for mRNA isolation, While A549 served as positive control for alveolar epithelial cell markers, hSMC was used as a negative control. Scale = 100x.

Supplementary Figure 5:

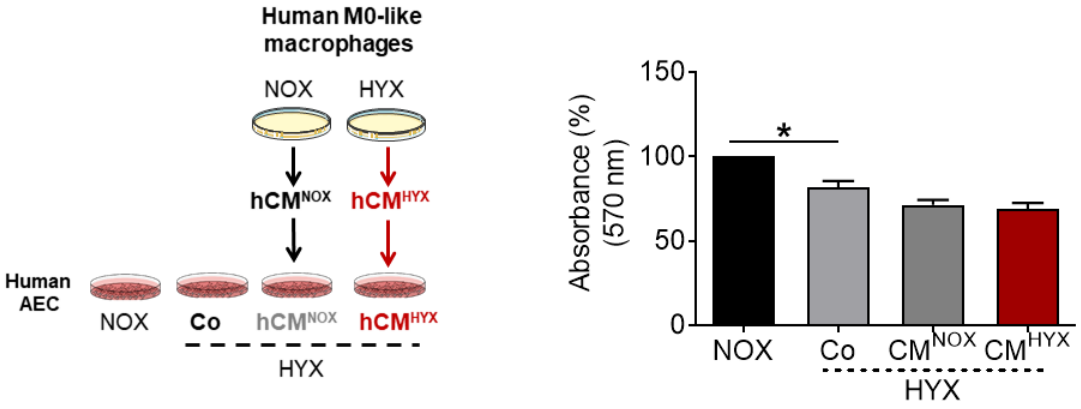

Supplementary Figure 5: Human M0-like macrophages were exposed to normoxia (21 % O_2, NOX) or 85 % O_2, HYX) for 48 h and conditioned media (CM) was collected. Subsequently, human alveolar epithelial cells (hAEC) were exposed to HYX and treated with CM of NOX-exposed M0-like macrophages (CM^{NOX}), CM^{HYX} or vehicle (medium, Co) for 24 h; Control hAEC were exposed to NOX. At the end of the experiment, proliferation of hAEC was assessed using MTT assay; n = 4 /group. Mean±SEM; n = 4-5/group; Paired t test: *$p<0.05$.